

Manuscript Information

Journal name: Molecular cell
NIHMS ID: NIHMS858018
Manuscript Title: PARK2 depletion connects energy and oxidative stress to PI3K/Akt activation via PTEN S-nitrosylation
Submitter: Author support, Elsevier (ElsevierNIHsupport@elsevier.com)

Manuscript Files

Type	Fig/Table #	Filename	Size	Uploaded
manuscript		MOLCEL_6171.pdf	7617361	2017-03-07 09:46:01
supplement	1	Supplemental Information.pdf	10047241	2017-03-07 09:46:25
supplement	2	Supplemental table 1.xlsx	49230	2017-03-07 09:46:25
supplement	3	Supplemental table 2.xlsx	51114	2017-03-07 09:46:25
citation		858018_cit.cit	127	2017-03-07 09:45:42

This PDF receipt will only be used as the basis for generating PubMed Central (PMC) documents. PMC documents will be made available for review after conversion. Any corrections that need to be made will be done at that time. No materials will be released to PMC without the approval of an author. Only the PMC documents will appear on PubMed Central -- this PDF Receipt will not appear on PubMed Central.

Accepted Manuscript

PARK2 depletion connects energy and oxidative stress to PI3K/Akt activation via PTEN S-nitrosylation

Amit Gupta, Sara Anjomani-Virmouni, Nikos Koundouros, Maria Dimitriadi, Rayman Choo-Wing, Adamo Valle, Yuxiang Zheng, Yu-Hsin Chiu, Sameer Agnihotri, Gelareh Zadeh, John M. Asara, Dimitrios Anastasiou, Mark J. Arends, Lewis C. Cantley, George Pouligiannis

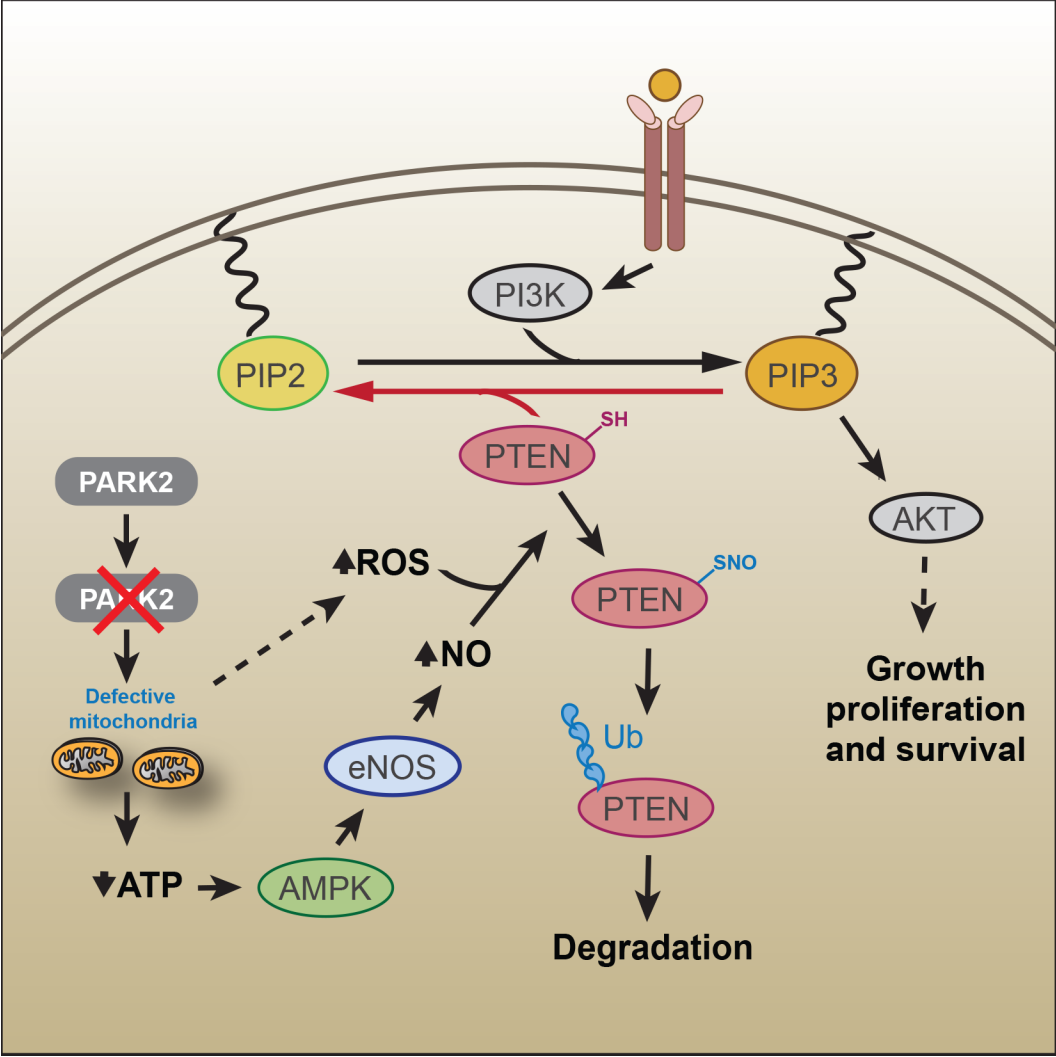
PII: S1097-2765(17)30134-X
DOI: doi:[10.1016/j.molcel.2017.02.019](https://doi.org/10.1016/j.molcel.2017.02.019)
Reference: MOLCEL 6171

Published in: *Molecular Cell*

Received date: 9 June 2016
Revised date: 13 December 2016
Accepted date: 17 February 2017

Cite this article as: Gupta A, Anjomani-Virmouni S, Koundouros N, Dimitriadi M, Choo-Wing R, Valle A, Zheng Y, Chiu Y-H, Agnihotri S, Zadeh G, Asara JM, Anastasiou D, Arends MJ, Cantley LC, Pouligiannis G, *PARK2* depletion connects energy and oxidative stress to PI3K/Akt activation via PTEN S-nitrosylation, *Molecular Cell*, doi:[10.1016/j.molcel.2017.02.019](https://doi.org/10.1016/j.molcel.2017.02.019)

This is a PDF file of an unedited manuscript that has been accepted for publication. As a service to our customers we are providing this early version of the manuscript. The manuscript will undergo copyediting, typesetting, and review of the resulting proof before it is published in its final citable form. Please note that during the production process errors may be discovered which could affect the content, and all legal disclaimers that apply to the journal pertain.



HIGHLIGHTS AND eTOC BLURB

- *PARK2* negatively regulates the PI3K/Akt pathway
- *PARK2* depletion promotes PTEN inactivation by S-nitrosylation and ubiquitination
- AMPK activation triggers PTEN S-nitrosylation in the absence of *PARK2* depletion
- *PARK2* and *PTEN* loss display striking cooperativity to promote tumorigenesis *in vivo*

Gupta et al. reveal an important missing piece in the dynamic signaling and metabolic network governing PI3K/Akt activation. *PARK2* inactivation connects energy and oxidative stress to Akt activation via redox-mediated inactivation of PTEN by S-nitrosylation to support cell survival under conditions of energy deprivation.

***PARK2* depletion connects energy and oxidative stress to PI3K/Akt activation via PTEN S-nitrosylation**

Amit Gupta¹, Sara Anjomani-Virmouni¹, Nikos Koundouros^{1,2}, Maria Dimitriadi^{1,3}, Rayman Choo-Wing⁴, Adamo Valle^{1,5}, Yuxiang Zheng⁶, Yu-Hsin Chiu⁷, Sameer Agnihotri⁸, Gelareh Zadeh⁸, John M. Asara⁹, Dimitrios Anastasiou¹⁰, Mark J. Arends¹¹, Lewis C. Cantley^{6,*}, George Poulgiannis^{1,2,12,*}

¹Signalling and Cancer Metabolism Team, Division of Cancer Biology, The Institute of Cancer Research, 237 Fulham Road, London, SW3 6JB, UK.

²Division of Computational and Systems Medicine, Department of Surgery and Cancer, Imperial College London, SW7 2AZ, UK.

³Department of Biological and Environmental Sciences, University of Hertfordshire, Hatfield, AL10 9AB, UK.

⁴Novartis Institutes for BioMedical Research, Inc., 181 Massachusetts Ave, Cambridge, MA 02139, USA.

⁵Energy Metabolism and Nutrition, University of Balearic Islands, Research Institute of Health Sciences (IUNICS) and Medical Research Institute of Palma (IdiSPa), Palma de Mallorca; Biomedical Research Networking Center for Physiopathology of Obesity and Nutrition (CIBERObn), Instituto de Salud Carlos III, Madrid, Spain.

⁶Meyer Cancer Center, Department of Medicine, Weill Cornell Medicine, New York, NY 10065, USA.

⁷Novartis Institutes for BioMedical Research, Inc., 22 Windsor Street, Cambridge, MA 02139, USA.

⁸MacFeeters-Hamilton Neurooncology Program, Princess Margaret Cancer Centre, Toronto, Canada.

⁹Division of Signal Transduction, Beth Israel Deaconess Medical Center, Boston, MA 02115, USA; Department of Medicine, Harvard Medical School, Boston, MA 02175, USA.

¹⁰Cancer Metabolism Laboratory, The Francis Crick Institute, London NW7 1AA, UK.

¹¹University of Edinburgh, Division of Pathology, Edinburgh Cancer Research Centre, Institute of Genetics & Molecular Medicine, Western General Hospital, Edinburgh, EH4 2XR, UK.

¹²Lead Contact

*Correspondence: lcantley@med.cornell.edu (L.C.C.), george.poulgiannis@icr.ac.uk (G.P.)

SUMMARY

PARK2 is a gene implicated in disease states with opposing responses in cell fate determination, yet its contribution in pro-survival signaling is largely unknown. Here, we show that *PARK2* is altered in over a third of all human cancers and its depletion results in enhanced PI3K/Akt activation, and increased vulnerability to PI3K/Akt/mTOR inhibitors. *PARK2* depletion contributes to AMPK-mediated activation of eNOS, enhanced levels of reactive oxygen species and a concomitant increase in oxidized nitric oxide levels, thereby promoting inhibition of PTEN by S-nitrosylation and ubiquitination. Notably, AMPK activation alone is sufficient to induce PTEN S-nitrosylation in the absence of *PARK2* depletion. *Park2* and *Pten* loss also display striking cooperativity to promote tumorigenesis *in vivo*. Together, our findings reveal an important missing mechanism that might account for PTEN suppression in *PARK2*-deficient tumors and highlight the importance of PTEN S-nitrosylation in supporting cell survival and proliferation under conditions of energy deprivation.

INTRODUCTION

Cell homeostasis is achieved through an orchestrated balance of cell signaling interactions that dictate the likelihood of a cell to escape from normal growth restraints or be eliminated from the replicative pool, resulting in cell death. Cancer is a group of diseases that are due to escape from cell death control, while Parkinson's disease (PD) portrays a disease that results from accelerated cell death. It would seem unlikely that these diseases are related, yet there is increasing evidence to suggest that a subset of PD susceptibility genes are also associated with cancer (Ong et al., 2014).

PARK2 was originally identified as a gene associated with the pathogenesis of familial PD in early-onset autosomal recessive juvenile Parkinsonism (Kitada et al., 1998). It has been reported to be mutated in as high as 77% of PD patients with an age of onset of <20 years, but only in 3% of patients with an age of onset of >30 years (Lucking et al., 2000). Subsequently, it has been linked with a wide range of disorders including leprosy (Mira et al., 2004), autism (Glessner et al., 2009), type 2 diabetes mellitus (Wongseree et al., 2009), Alzheimer's disease (Burns et al., 2009), cerebellar ataxia (Periquet et al., 2003), resistance to intracellular pathogen infections (Manzanillo et al., 2013) and cancer, where it is somatically deleted in a wide spectrum of tumor types (Bernardini et al., 2016). *PARK2* is a *bona fide* haploinsufficient tumor suppressor, as depletion of a single *PARK2* allele significantly increases adenoma development and polyp multiplicity in *Apc^{Min/+}* mice (Poulogiannis et al., 2010). *PARK2* loss also renders mice more susceptible to hepatocellular (Fujiwara et al., 2008) and γ -irradiation induced carcinomas (Zhang et al., 2011), while ectopic *PARK2* expression mitigates cell proliferation in colorectal, glioma, breast, hepatocellular, and non-small cell lung cancer cells (Lin et al., 2015; Picchio et al., 2004; Poulogiannis et al., 2010; Tay et al., 2010; Veeriah et al., 2010; Wang et al., 2004; Yeo et al., 2012).

The *PARK2* gene encodes the E3 ubiquitin ligase Parkin, which mediates the ubiquitination of a number of substrate proteins, leading to their proteasomal degradation (Dawson and Dawson, 2010). Its activities go beyond the degradative ubiquitination and it is implicated in the regulation of multiple cellular processes including stress response, mitochondrial biogenesis and stability of G1/S cyclins (Corti and Brice, 2013; Gong et al., 2014). Although the underlying mechanisms by which pathogenic *PARK2* mutations contribute to PD are not entirely understood, mitochondrial dysfunction is considered to play a central role in stress-induced neuronal cell death associated with the pathogenesis of this disorder. Increased oxidative and nitrosative stress is a common phenomenon in both PD and cancer, hence it is imperative to identify the molecular pathways underlying the functional contribution of *PARK2* depletion in these processes.

Compelling evidence shows that cancer cells utilize multiple pathways including the phosphatidylinositol 3-kinase/Akt (PI3K/Akt) signaling pathway to enhance their survival and prevent apoptosis under metabolic stress conditions (Trachootham et al., 2008). Importantly, *PARK2* has previously been associated with the activation of the Akt pathway (Fallon et al., 2006; Lin et al., 2015; Yeo et al., 2012), however the mechanistic evidence behind its functional contribution is unclear. One study showed that Parkin interacts with and ubiquitinates Eps15 to delay the internalization and degradation of its adaptor protein EGFR, thereby promoting PI3K/Akt signaling (Fallon et al., 2006), while a more recent study suggests that Parkin directly interacts with and promotes the ubiquitination of EGFR, leading to diminished activation of EGF-induced PI3K/Akt signaling (Lin et al., 2015). These data highlight the need for further investigation of the molecular events underlying the role of *PARK2* depletion in PI3K/Akt-mediated cellular survival.

In this study, we identified PTEN as an important mediator behind the functional contribution of *PARK2*-depletion in the activation of the PI3K/Akt pathway, and further characterized its pivotal role in the tumor suppressor function of *PARK2* in

vitro and *in vivo*. Additionally, our results reveal an important missing piece in the dynamic signaling and metabolic network connecting AMPK with Akt activation in the absence of mTORC1-S6K-dependent negative feedback loop mechanisms (Efeyan and Sabatini, 2010), demonstrating a compensatory survival mechanism for cancer cells under conditions of energy deprivation.

RESULTS

***PARK2* genomic and gene expression profiling across human cancers**

We examined the degree of *PARK2* deletion on the largest up-to-date collection of The Cancer Genome Atlas (TCGA) assembling data from 9,863 primary tumors from 28 different tumor types (**Table S1**). Focal deletions (dark blue; **Figure 1A**) of the *PARK2* gene were most commonly found in colorectal (21%) and ovarian (25%) carcinomas, while a strikingly high number of tumors including lung adenocarcinomas, melanomas, bladder, ovarian and pancreatic had an overall >40% DNA copy number (DCN) loss of the *PARK2* gene [both focal deletion (dark blue) and as part of whole or part chromosome arm losses (light blue), **Figure 1A**]. Cholangiosarcomas (CHO) showed a staggering 69% (25/36) rate of overall *PARK2* deletions. In parallel, we also examined the degree of *PARK2* mRNA decrease between cancer and corresponding normal tissues from a total number of 13,481 specimens, studied in 127 published microarray datasets (**Table S2**), covering 25 tumor types. Notably, there are many cancer types including gliomas, cervical, and kidney carcinomas with not the highest frequency of overall *PARK2* deletion (<40%), but with widespread (up to 69%) decrease or loss of its mRNA expression compared to their normal counterparts (>1 log₂ fold, red or >0.5 log₂ fold, red and yellow; **Figure 1B, S1A**). Vice versa there are some tumor types e.g. ovarian cancer, where *PARK2* deletion is found in >60% of the cases, yet only a small fraction are reported to have low *PARK2* mRNA expression. This reflects in part the stringent criteria we used to report tumor types with >0.5 fold changes in mRNA expression compared to their normal counterparts, but also that the majority (>90%) of *PARK2* deletions across all tumor types are heterozygous, hence are less likely to cause a marked reduction in *PARK2* mRNA expression.

As high as 2/3 of glioma tumors have significantly reduced levels of *PARK2* mRNA expression compared to their corresponding normal (**Figure 1B**). We plotted the distribution of *PARK2* expression across different subgroups of gliomas reminiscent of distinct neural cell types, to show that *PARK2* is significantly downregulated irrespectively of the histological origin of this tumor type (**Figure S1B**). To identify relationships between *PARK2* DCN and mRNA expression levels, we plotted the distribution of its expression across subgroups of glioblastomas (GBMs) with different *PARK2* DCN. *PARK2* mRNA expression is progressively lower across the different subgroups of *PARK2* ploidy status (**Figure 1C**). To assess the prognostic significance of this gene across different types of genetic alteration, we also performed survival analysis between subgroups of patients with GBM divided based on different molecular markers of the *PARK2* gene. Interestingly, loss of *PARK2* at the DNA, mRNA and protein levels (**Figure 1D**) all correlate with significantly poorer survival in patients with GBM (**Figure 1E**). Of note, *PARK2* expression is also associated with poorer survival in patients with breast and lung adenocarcinomas (**Figure S1C-D**). Collectively, our data demonstrate that *PARK2* is altered in over a third of all human cancers. Its widespread loss or decrease across many molecular biomarker indicators (DNA, mRNA, protein) significantly correlates with poorer survival offering great prognostic and predictive value for clinical practice.

***PARK2* regulates the activation of the PI3K/Akt pathway**

The PI3K/Akt pathway is the single most frequently altered signaling cascade across all the tumor types with recurrent *PARK2* deletions and mRNA loss/reduction (Yuan and Cantley, 2008). Activation of the PI3K/AKT/mTOR pathway has also been associated with significantly poorer survival across many solid tumors (Ocana et al., 2014). To investigate whether activation of this pathway is inherently associated with loss of the *PARK2* gene, we stably expressed two independent hairpins targeted against *PARK2* in HCT116 cells. Cells with *PARK2* knockdown exhibited a pronounced increase in Akt phosphorylation compared to control GFP knockdown

cells (**Figure 2A**). Staurosporine is a protein kinase inhibitor that can induce apoptosis across many different cell types and Akt hyperactivation has been shown to attenuate sensitivity to staurosporine-induced cell death (Mookherjee et al., 2007). We showed that *PARK2* depletion augmented resistance to staurosporine-induced cell death (**Figure 2B**) and this was consistent with significantly lower apoptotic response as indicated by Caspase 3/7 activity (**Figure 2C**).

Identification of candidate biomarkers that predict responsiveness to specific signaling cascade inhibitors is increasingly important in the era of personalized medicine. Accordingly, we assessed the role of *PARK2* knockdown to the inhibition of various signaling nodes across the PI3K/Akt/mTOR and MAPK pathways. *PARK2* depletion renders cells more sensitive to inhibitors of PI3K (BKM120 and BEZ235), Akt (MK2206), and mTOR (BEZ235, Rapamycin and Torin), but it decreases the effectiveness of MEK inhibitors PD0325901 and GSK1120212 (**Figure 2D-E, S2A-B**). Taken together, these data suggest that *PARK2* loss contributes in the activation of Akt signaling and the dependence of cells on this pathway, suggesting that *PARK2* deficiency could be used as a biomarker of efficacy and favorable clinical response to inhibitors of the PI3K/Akt/mTOR pathway.

***PARK2* suppresses Akt activation and tumorigenicity in *PTEN* wild-type, but not *PTEN* mutant cells**

To explore the significance of Akt activation in the molecular mechanisms that *PARK2* may contribute to tumor suppression, we tested the effect of *PARK2* overexpression in *PTEN* wild type (WT) (HCT116 *PTEN*^{+/+} and H1299) and *PTEN* mutant (PC3 and HCT116 *PTEN*^{-/-}) cell line models. Ectopic expression of *PARK2* led to inhibition of Akt phosphorylation in HCT116 cells (**Figure 3A**). Importantly, we showed that *PARK2* overexpression led to inhibition of Akt activation upon growth factor stimulation in *PTEN* WT H1299 cells (**Figure 3B**), but not in the *PTEN* mutant PC3 cells (**Figure 3C**). This reduction in Akt phosphorylation was also apparent when we ectopically expressed *PARK2* at levels near the endogenous Parkin levels expressed in H460 cells, for both the *EGFR* WT (H1299) and *EGFR* null (SW620) cells (**Figure S2C-D**). Unlike in parental *PTEN*^{+/+} HCT116 cells, overexpression of *PARK2* did not reduce Akt phosphorylation in isogenic *PTEN*^{-/-} HCT116 cells (**Figure S2E**), further supporting a role for *PTEN* in *PARK2*-mediated regulation of PI3K/Akt signaling.

Akt has been shown to play a central role in promoting growth factor-mediated cell proliferation and migration (Manning and Cantley, 2007). Given that *PARK2* inhibits Akt phosphorylation, we sought to investigate its functional contribution in suppressing some of the cellular functions mediated by Akt activation. HCT116 *PTEN*^{+/+} and H1299 cells exhibited a pronounced reduction in both cell proliferation (**Figure 3D**) and cell migration (**Figure 3E**) upon *PARK2* overexpression. However, this was not true for the *PTEN* mutant, PC3 and isogenic *PTEN*^{-/-} HCT116 cells that showed no effect compared to control empty-vector (EV) expressing cells. No effect on cell proliferation and migration was also observed when overexpressing the E3-Ligase dead C431S Parkin mutant in both *PTEN* WT and mutant cells (**Figure S2F-H**).

To investigate the tumor suppressor effect of *PARK2* *in vivo*, we retro-orbitally injected luciferase labeled H1299 cells overexpressing EV or human *PARK2*. Ectopic expression of *PARK2* significantly mitigated the formation of lung metastases (**Figure 3F-I**) in NOD/SCID mice. The luciferase activity in cells expressing the *PARK2* gene was reduced on both week 3 and 4 post-injection (**Figure 3F-G**), and this was consistent with significantly lower number and smaller size of lung metastases, as histopathologically evaluated with H&E-stained sections (**Figure 3H-I**). These data show that suppression of Akt activation plays a central role in the tumor suppressor function of *PARK2*, and that the mutational status of *PTEN*

determines the functional contribution of *PARK2* loss in Akt-mediated cell proliferation and migration.

***PARK2* depletion suppresses PTEN protein levels and activity**

To further investigate the role of PTEN in *PARK2*-mediated regulation of the PI3K/Akt pathway, we performed *PARK2* knockdown analysis in cell lines with abundant Parkin, but either WT *PTEN* present (HCT116 and H460) or absent (PC3 and U138). In line with our overexpression studies, *PARK2* knockdown induced Akt phosphorylation in HCT116 and H460 cells, but not in PC3 or U138 cells (**Figure 4A, S3A-B**) or in the isogenic *PTEN*-null HCT116 (**Figure 4B**) and MCF10A cells (**Figure S3C**). Most importantly, *PARK2* depletion led to a >30% reduction in PTEN protein levels across all *PTEN* WT cell lines (**Figure 4A-B, S3C**) and this observation was confirmed in CRISPR/Cas9-mediated *PARK2* knockout H460 cells (**Figure S3D**). Previous studies with hypomorphic *Pten* allelic series of mice have shown that even subtle reductions in *Pten* protein levels can have dramatic consequences in cancer progression (Trotman et al., 2003). PTEN is regulated in cancer at the transcriptional, post-transcriptional and post-translational levels (Song et al., 2012). To further gain insight into this regulation by *PARK2*, we performed qPCR analysis of both *PARK2* and *PTEN* following lentiviral knockdown of *PARK2* and showed that *PARK2* depletion does not affect *PTEN* mRNA levels (**Figure 4C, S3E**). Importantly, *PARK2* depletion resulted in a significantly lower PTEN enzymatic activity (**Figure 4D, S3F**) and higher levels of PI(3,4,5)P₃ and PI(3,4)P₂ in cells (**Figure 4E**), further supporting the functional contribution of PTEN in *PARK2*-mediated regulation of the PI3K/Akt pathway. Moreover, we were struck to observe a reciprocal correlation between Parkin and PTEN protein expression across ten breast cancer cell lines that have previously been reported to be WT for *PTEN* (**Figure S3G**) (Saal et al., 2008). In view of our findings, we speculated that suppression of PTEN protein levels by *PARK2* depletion might be regulated by proteasome-mediated protein degradation. Indeed, treatment with proteasome inhibitor MG132 led to an overall increase in PTEN protein levels and no significant difference between *GFP* and *PARK2*-knockdown cells (**Figure 4F, S3H**). Taken together, these results showed that *PARK2* depletion suppresses PTEN protein levels and activity and raised an interesting hypothesis that mechanistically, this could be regulated, at least in part, by ubiquitin proteasome-mediated protein degradation.

Increased oxidative and nitrosative stress upon *PARK2* depletion

Recent evidence shows that Parkin loss leads to a marked decrease in mitochondrial biogenesis (Stevens et al., 2015). To investigate the role of *PARK2* depletion in cellular metabolism, we initially measured the effect of knocking down *PARK2* expression on the oxygen consumption rate (OCR) of shGFP- and sh*PARK2*-expressing cells in the presence or absence of different mitochondrial stress inhibitors, using the Seahorse XFe96 Flux Analyser. Notably, *PARK2* depletion resulted in a marked decrease in basal, maximal, mitochondrial and non-mitochondrial respiration (**Figure 5A-B, S4A-B**).

We next explored the effects of *PARK2* depletion on cellular metabolism by performing targeted metabolomic analysis. Consistent with lower OCR levels, *PARK2* knockdown cells showed a significant decrease in ATP levels (**Figure 5C**) and a concomitant activation of AMPK (**Figure 5D, Figure S4C**), accompanied by the inhibition of mTORC1 signaling (**Figure S4D-E**). *PARK2* depletion also caused a reduction across many of the cofactors that contribute in nitric oxide (NO) biosynthesis, involving the conversion of L-arginine to L-citrulline (**Figure 5E-F**). Importantly, although all the anaplerotic substrates for NO synthesis were detected to be lower in the *PARK2* knockdown cells, L-citrulline levels were not significantly lower. Although other interpretations are possible, these results are consistent with a model in which NOS is activated due to loss of *PARK2* such that the substrates for

NOS are being consumed at a high rate, while the product of NOS L-citrulline is maintained at a relatively constant level. Indeed, consistent with this model, we measured the NOS activity and oxidized NO (NO_2+NO_3) levels and found that they are significantly higher in *PARK2* knockdown cells (**Figure 5G-H, S4F**). The latter also showed an overall increase in NADP/NADPH ratio (**Figure 5I**), higher ROS levels upon menadione treatment (**Figure 5J, S4G**), and lower reduced/oxidized glutathione (GSH/GSSG) levels (**Figure 5K, S4H**) compared to *GFP* control knockdown cells. Importantly, besides its function as a regulator of cellular redox status, GSH has a crucial role in modulating NO reactivity (Aquilano et al., 2014). NO as a free radical is a poor oxidant, hence NO-dependent cysteine oxidation primarily occurs in the presence of oxygen or high ROS (Broniowska and Hogg, 2012). Of note, we showed that GSH-MEE treatment restored the suppression in PTEN protein levels observed in *PARK2* knockdown cells (**Figure 5L, S4I**), while BSO treatment further enhanced the reduction in PTEN (**Figure S4J**). In addition, the activity of PTEN in *PARK2* knockdown cells in the presence of DTT was comparable to the sh*GFP* cells without the DTT pre-incubation (**Figure S4K**), reinforcing the conclusion that the inhibition of PTEN is generated by a redox-dependent modification of cysteine residues.

Mitochondrial dysfunction and oxidative stress are well-recognized mechanisms leading to the activation of AMPK that can directly phosphorylate endothelial NOS (eNOS) to increase its catalytic activity (Schulz et al., 2009). In line with this, we showed that *PARK2* knockdown (**Figure S4L**) or allosteric activation of AMPK following treatment with the small molecule activator 991 (**Figure 5M**) led to an increase of eNOS phosphorylation and a reduction in PTEN protein levels. Of note, this reduction in PTEN protein levels and concomitant increase in Akt activation that was observed in 991-treated cells were decreased upon co-treatment with the NO scavenger cPTIO (**Figure S4M**). Collectively, these results demonstrate that *PARK2* depletion leads to mitochondrial dysfunction, high eNOS activity that is mediated, at least in part, by AMPK activation and high ROS levels that together coordinate efficient NO oxidation.

***PARK2* depletion promotes PTEN S-nitrosylation and ubiquitination**

High NO production exerts a pleiotropic range of biological functions that are regulated in part, by a post-translational redox-mediated modification known as S-nitrosylation of protein cysteine residues. PTEN has previously been identified as a target of such modification (Kwak et al., 2010; Numajiri et al., 2011) that leads to the inhibition of its enzymatic activity and downstream activation of Akt signaling. In view of our previous findings, we speculated that *PARK2* depletion-mediated activation of the Akt pathway might be regulated by PTEN S-nitrosylation. Indeed, *PARK2* depletion resulted in a marked induction of PTEN S-nitrosylation (SNO-PTEN), as indicated both by immunoblotting immunoprecipitated PTEN with the anti-S-nitrosocysteine antibody (**Figure 6A, S5B**), as well as by measuring the release of NO from S-nitrosothiol of recombinant PTEN using the quantitative fluorescent 2,3-diaminonaphthalene (DAN) assay (**Figure 6B, S5C**). Interestingly, PTEN S-nitrosylation has previously shown to promote its ubiquitination (Kwak et al., 2010), which could also explain the reduction in total PTEN protein levels and rescue following treatment with the proteasome inhibitor MG132 (**Figure 4F, S3H**). We performed in-cell PTEN ubiquitination assay and showed that *PARK2* depletion resulted in a marked increase in PTEN ubiquitination with or without pre-treatment with MG132 for 6 hours (**Figure 6C-D, S5D**). Consistent with enhanced PTEN ubiquitination, we also found an increased abundance of conjugated ubiquitin (ub) on PTEN in *PARK2* knockdown HCT116 cells expressing HA-Ubiquitin (**Figure S5A**). An increase in phospho-Akt levels was observed in MG132-treated cells even in the absence of *PARK2* knockdown (**Figure 6C**), perhaps reflecting the increase in ub

conjugates and PTEN ubiquitination (**Figure 6D**) resulting from proteasome inhibition.

Cysteine (Cys-83) has previously been identified as the critical cysteine thiol group within PTEN's phosphatase domain that is predominantly targeted for S-nitrosylation, and in line with this, C83S mutant PTEN is resistant to modification (Numajiri et al., 2011). Accordingly, we overexpressed WT and C83S mutant PTEN in the presence or absence of *PARK2* lentiviral shRNA to show that the C83S mutant was completely devoid of S-nitrosylation and rescued Akt activation in *PARK2* knockdown cells (**Figure 6E**). Importantly, since the activation of eNOS is also regulated by Akt-dependent phosphorylation (Dimmeler et al., 1999), our observation raised a dilemma whether the contribution of *PARK2* depletion to PTEN inhibition by S-nitrosylation is the consequence of Akt activation or is regulated via AMPK-mediated activation of eNOS independently of PI3K-Akt. To address this we treated shGFP- and sh*PARK2*-expressing HCT116 with the Akt inhibitor MK-2206 to show that inhibition of Akt activity does not rescue S-nitrosylation of PTEN (**Figure S5E**), nor the increased NO levels in *PARK2* knockdown cells (**Figure S5F**). On the contrary, siRNA-mediated down-regulation of *AMPK* (*AMPK* α 1 and α 2) led to a reduction in PTEN S-nitrosylation in *PARK2* knockdown cells (**Figure 6F**), further supporting the mechanistic implication of AMPK in *PARK2*-mediated activation of Akt.

To determine the importance of AMPK activation to trigger PTEN S-nitrosylation, we tested if AMPK activation alone is sufficient to induce this modification in the absence of *PARK2* depletion. Activation of AMPK following 991 treatment, glucose deprivation or oligomycin treatment all led to a marked increase in PTEN S-nitrosylation (**Figure 6G**), identifying a functional cross-talk between AMPK and Akt activation.

To better understand the physiological importance of PTEN S-nitrosylation in the proliferation and survival of cells under conditions of metabolic stress, we performed clonogenic assays in *PTEN* null PC3 cells overexpressing EV, WT or SNO-resistant (C83S) PTEN in the presence or absence of the glycolysis inhibitor 2-Deoxy-D-glucose (2-DG). Although no significant difference in colony formation was detected in *PTEN*-WT overexpressing cells with or without 2-DG treatment, there was a marked reduction (~30%) in the number of colonies following 2-DG treatment in PC3 cells with enforced expression of the C83S mutant PTEN (**Figure S6A-C**). Moreover, we compared the half maximal inhibitory concentrations (IC₅₀s) of 2-DG or dichloroacetate (DCA) (PDK inhibitor), both of which result in the activation of AMPK in response to ATP depletion, to show that PC3 cells expressing the C83S mutant exhibited significantly higher sensitivity to treatment with these drugs, not evident in *PTEN* WT-expressing PC3 cells (**Figure S6D-E**). Last but not least, and consistent with the ability of *PARK2* knockdown cells to inactivate WT PTEN, we showed that sh*PARK2* cells proliferate significantly faster than shGFP-expressing cells in the presence of ectopic co-expression of WT (**Figure S6F**), but not C83S mutant PTEN (**Figure S6G**). Taken together, these data demonstrate that *PARK2* depletion contributes to the activation of Akt signaling through promoting S-nitrosylation and ubiquitination of the tumor suppressor *PTEN*. Notably, our data also highlight a previously unexplored mechanism contributing to AMPK-mediated activation of PI3K/Akt involving the inhibition of PTEN by S-nitrosylation, which appears to be critical for the proliferative capacity and survival of *PTEN*-proficient cancer cells under conditions of energy stress.

***Park2* deletion dramatically promotes tumorigenesis in *Pten* heterozygous knock-out mice**

Given the functional contribution of *PARK2* depletion in PTEN inactivation by S-nitrosylation, we performed a bioinformatic analysis to report the copy number alterations (CNAs) of *PARK2* and *PTEN* across 995 cancer cell lines of the Cancer Cell Line Encyclopedia (CCLE) project. We were struck to identify that almost 1/2 cell lines with HET deletion in *PTEN* (n=145/314, 46.2%) also have HET deletion in

PARK2, with the coexistence for LOH at both the *PTEN* and *PARK2* loci being far more frequent than *PTEN* (n=79/314, 25.2%) or *PARK2* (n=119/344, 34.6%) LOH alone (**Figure S7A**). We extended this bioinformatic analysis summarizing the percentage of *PARK2* CNAs of primary tumors or cancer cell lines with *PTEN* LOH on 1,953 specimens across 13 different cancer types from the TCGA database to show that there is a strong selection for *PARK2* LOH, when one copy of the *PTEN* gene is missing (**Figure S7B**).

In an effort to study whether *Park2* loss further exacerbates *Pten*-mediated tumorigenesis *in vivo*, mice with a targeted knockout of *Park2* exon 3 (Itier et al., 2003) were crossed with *Pten*^{+/-} mice (Di Cristofano et al., 1998). The latter are born viable and develop prostatic intraepithelial neoplasia (PIN), as well as numerous neoplastic lesions in many organs including skin, colon, endometrium, liver, thyroid, and thymus (Di Cristofano et al., 1998; Podsypanina et al., 1999). Although, *Pten*^{+/-}/*Park2*^{+/-} and *Pten*^{+/-}/*Park2*^{-/-} mice showed a similar spectrum of tumors like the ones detected in *Pten*^{+/-}/*Park2*^{+/+} mice, they were significantly more tumor prone and exhibited features reminiscent of mice with a hypomorphic and a knockout *Pten* allele (**Figure 7A**). *Park2* loss was associated with an increased incidence of high-grade PIN and low-grade prostate adenocarcinoma (**Figure 7B, 7D**), as well as significantly higher numbers of solid thyroid adenocarcinomas (**Figure 7C**). Most importantly, mice bearing *Park2* loss developed tumor types including hystiocytic sarcoma, multiple myeloma and osteosarcoma in spine (**Figure S7C-D**) that have not been previously described for the *Pten*^{+/-} mice. On two occasions, mice bearing both *Park2* and *Pten* loss developed malignant pheochromocytomas and thyroid adenocarcinomas that metastasized to the lung (**Figure S7C-D**). As a result, *Pten*^{+/-}/*Park2*^{+/-} and *Pten*^{+/-}/*Park2*^{-/-} mice showed significantly poorer survival compared to *Pten*^{+/-}/*Park2*^{+/+} mice (**Figure 7E-F**), while no difference in relative survival was found between *Pten*^{+/-}/*Park2*^{+/-} and *Pten*^{+/-}/*Park2*^{-/-} mice (**Figure S7E**).

To further assess the contribution of the proposed model on the *PARK2*-mediated inactivation of *PTEN in vivo*, we performed immunohistochemical (IHC) analysis of *PTEN* and phospho-Akt on tumor sections derived from *Pten*^{+/-} mice bearing WT, heterozygous (HET) or homozygous (HOM) deletion in *Park2*. Consistent with reduced *PTEN* and elevated phospho-Akt expression observed in the immunoblot analyses, *Pten*^{+/-} tumor epithelia bearing one or no copies of *Park2*, expressed no or low *PTEN* protein levels and showed significantly higher phospho-Akt staining compared to lesions in *Pten*^{+/-}/*Park2*^{+/+} mice (**Figure S7F-H**). Overall, our analysis showed that loss of function of *Park2* and *Pten* displayed striking cooperativity to promote tumorigenesis and significantly shorten tumor-free survival.

DISCUSSION

The PI3K/Akt pathway represents a complex signaling network that integrates numerous upstream stimuli to regulate diverse cellular processes, including cell growth, proliferation, survival, and migration (Manning and Cantley, 2007). Interestingly, the *PARK2* gene is associated with the pathogenesis of disease states that are characterized by different responses in cell fate determination, therefore understanding its functional contribution in the activation of survival pathways is clearly of immense clinical benefit.

In this study, we identify a PTEN-mediated role for *PARK2* depletion in the activation of the PI3K/Akt pathway. Of note, recent evidence suggested that *PARK2* interacts with EGFR to promote its ubiquitination, thereby inhibiting Akt activation (Lin et al., 2015). However the role of EGFR in *PARK2*-mediated activation of PI3K-Akt signaling might be more complex and/or cell-type specific than previously appreciated, as ectopic *PARK2* expression suppresses Akt activation even in EGFR-null SW620 cells.

PTEN is a well-characterized haploinsufficient tumor suppressor (Di Cristofano et al., 1998), yet emerging evidence suggests that its function goes beyond its tumor suppressor role, as a critical regulator of multiple central nervous system functions (Ismail et al., 2012). *PTEN* loss and subsequent activation of the PI3K/Akt signaling promotes the activation of mTOR signaling, which is hyperactive in many cancers (Carracedo and Pandolfi, 2008). Notably, inhibition of mTORC1 by rapamycin treatment prevents PD symptoms in mice bearing a human mutation in the *PARK2* gene (Siddiqui et al., 2015). Furthermore, *PTEN* loss leads to downregulation of PINK1 expression (Unoki and Nakamura, 2001) supporting a mechanism to suggest that *PARK2* LOH could repress PINK1 through inactivating PTEN, and PINK1 repression could obliterate any residual activity of the remaining *PARK2* allele, by abrogating Parkin translocation to mitochondria.

An important mode of NO function primarily involves its reaction with oxygen or ROS and subsequent oxidation to nitrogen dioxide (NO₂), dinitrogen trioxide (N₂O₃), or peroxynitrite (ONOO⁻), which ultimately lead to nitrosative stress and S-nitrosylation of target proteins and other biomolecules (Kovacs and Lindermayr, 2013). Of note, NO signaling and S-nitrosylation has previously been detected to contribute to PTEN inactivation in neurodegeneration (Kwak et al., 2010), but its role in cancer has been largely unknown. In this study, we showed that one of the most common genetic alterations across human cancers - *PARK2* loss, contributes to S-nitrosylation of PTEN, thereby promoting its ubiquitin-dependent degradation by the proteasome. We also report that there is a strong selection for co-occurrence of *PARK2* and *PTEN* LOH in cancer. This suggests that the high incidence of complete IHC loss of PTEN in *PTEN* HET tumors could be explained, at least in part, due to *PARK2* LOH, leading to S-nitrosylation and ubiquitination of the protein encoded from the remaining *PTEN* allele. In line with our previous observations (Poulogiannis et al., 2010), *PARK2* has many of the properties of a haploinsufficient tumor suppressor in that loss of a single *Park2* allele exacerbates tumorigenesis without requiring complete inactivation of the remaining allele.

Notably, activation of AMPK alone can trigger a marked increase in PTEN S-nitrosylation, pointing to a functional cross-talk between AMPK and Akt activation in the absence of any mTORC1-dependent negative feedback loop mechanisms (Efeyan and Sabatini, 2010). This redox-dependent modification in PTEN is important for supporting the survival and proliferative capacity of energy deprived cancer cells, signifying an important compensatory role for AMPK to support cell homeostasis via PTEN-mediated activation of Akt signaling. Further studies are needed to determine the physiological functions of enhanced NO signaling across different disease states, but the reaction between NO and PTEN forms a nexus that opens up unique therapeutic opportunities for targeting dysregulated protein S-

nitrosylation for a substantial fraction of tumors growing under conditions of energy deprivation.

AUTHOR CONTRIBUTIONS

G.P., and L.C.C. designed the study and wrote the manuscript. G.P., A.G., S.A.V, N.K., M.D., A.V., Y.Z., YH.C., and D.A. performed molecular biology experiments. S.A. and G.Z. performed Parkin IHC in GBM tumors. M.J.A. analyzed histopathology data. G.P. and J.M.A. performed metabolomics and analyzed the data. G.P. and R.CW. performed retro-orbital injection experiments and contributed to mouse colony management. G.P. performed bioinformatics analysis. All authors commented on the manuscript.

CONFLICT OF INTEREST

L.C.C. owns equity in, receives compensation from and serves on the Board of Directors and Scientific Advisory Board of Agios Pharmaceuticals. Agios Pharmaceuticals is identifying metabolic pathways in cancer cells and developing drugs to inhibit such enzymes to disrupt tumor cell growth and survival. No potential conflicts of interest were disclosed by the other authors.

ACKNOWLEDGEMENTS

We thank Rodrick Bronson, the entire HMS Rodent Histopathology Core and the ICR Pathology Core for technical help with the mouse histopathology and discussions concerning the project. We also thank David Carling for the generous gift of the 991 activator, Nick Leslie for the pHR-SIN-PTEN-WT and Tina Yuan for the pLV430G-oFL-T2A-eGFP vectors, Pier Paolo Pandolfi for giving us access to *Pten* KO mice, and Olga Corti and Alexis Brice for providing *Park2* KO mice. We thank Susanne Breitkopf and Min Yuan for help with mass spectrometry. This work was supported by grants from the NIH P01-CA120964 (J.M.A. and L.C.C.) and R01-GM041890. A.V. was funded by the Ministry of Education, Culture and Sport under the Program for Promoting and Hiring of Talent and its Employability (Subprogram for Mobility) of the Spanish Government. G.P. is funded by the ICR. Work in the D.A. lab is supported by MRC grant MC_UP_1202/1. Finally, we would like to dedicate this work to the memory of Professor Chris Marshall who was an esteemed colleague and mentor, whose scientific discoveries will continue to inspire us and translate basic science into benefits for cancer patients.

REFERENCES

Agnihotri, S., Gajadhar, A.S., Ternamian, C., Gorlia, T., Diefes, K.L., Mischel, P.S., Kelly, J., McGown, G., Thorncroft, M., Carlson, B.L., *et al.* (2012). Alkylpurine-DNA-N-glycosylase confers resistance to temozolomide in xenograft models of glioblastoma multiforme and is associated with poor survival in patients. *The Journal of clinical investigation* 122, 253-266.

Aquilano, K., Baldelli, S., and Ciriolo, M.R. (2014). Glutathione: new roles in redox signaling for an old antioxidant. *Frontiers in pharmacology* 5, 196.

Bernardini, J.P., Lazarou, M., and Dewson, G. (2016). Parkin and mitophagy in cancer. *Oncogene*.

Broniowska, K.A., and Hogg, N. (2012). The chemical biology of S-nitrosothiols. *Antioxidants & redox signaling* 17, 969-980.

Burns, M.P., Zhang, L., Rebeck, G.W., Querfurth, H.W., and Moussa, C.E. (2009). Parkin promotes intracellular Abeta1-42 clearance. *Human molecular genetics* 18, 3206-3216.

Carracedo, A., and Pandolfi, P.P. (2008). The PTEN-PI3K pathway: of feedbacks and cross-talks. *Oncogene* 27, 5527-5541.

Corti, O., and Brice, A. (2013). Mitochondrial quality control turns out to be the principal suspect in parkin and PINK1-related autosomal recessive Parkinson's disease. *Current opinion in neurobiology* 23, 100-108.

Dawson, T.M., and Dawson, V.L. (2010). The role of parkin in familial and sporadic Parkinson's disease. *Movement disorders : official journal of the Movement Disorder Society* 25 Suppl 1, S32-39.

Di Cristofano, A., Pesce, B., Cordon-Cardo, C., and Pandolfi, P.P. (1998). Pten is essential for embryonic development and tumour suppression. *Nature genetics* 19, 348-355.

Dimmeler, S., Fleming, I., Fisslthaler, B., Hermann, C., Busse, R., and Zeiher, A.M. (1999). Activation of nitric oxide synthase in endothelial cells by Akt-dependent phosphorylation. *Nature* 399, 601-605.

Efeyan, A., and Sabatini, D.M. (2010). mTOR and cancer: many loops in one pathway. *Curr Opin Cell Biol* 22, 169-176.

Fallon, L., Belanger, C.M., Corera, A.T., Kontogiannea, M., Regan-Klapisz, E., Moreau, F., Voortman, J., Haber, M., Rouleau, G., Thorarinsdottir, T., *et al.* (2006). A regulated interaction with the UIM protein Eps15 implicates parkin in EGF receptor trafficking and PI(3)K-Akt signalling. *Nature cell biology* 8, 834-842.

Fujiwara, M., Marusawa, H., Wang, H.Q., Iwai, A., Ikeuchi, K., Imai, Y., Kataoka, A., Nukina, N., Takahashi, R., and Chiba, T. (2008). Parkin as a tumor suppressor gene for hepatocellular carcinoma. *Oncogene* 27, 6002-6011.

Glessner, J.T., Wang, K., Cai, G., Korvatska, O., Kim, C.E., Wood, S., Zhang, H., Estes, A., Brune, C.W., Bradfield, J.P., *et al.* (2009). Autism genome-wide copy number variation reveals ubiquitin and neuronal genes. *Nature* 459, 569-573.

- Gong, Y., Zack, T.I., Morris, L.G., Lin, K., Hukkelhoven, E., Raheja, R., Tan, I.L., Turcan, S., Veeriah, S., Meng, S., *et al.* (2014). Pan-cancer genetic analysis identifies PARK2 as a master regulator of G1/S cyclins. *Nature genetics* 46, 588-594.
- Green, S., Trejo, C.L., and McMahon, M. (2015). PIK3CA(H1047R) Accelerates and Enhances KRAS(G12D)-Driven Lung Tumorigenesis. *Cancer research* 75, 5378-5391.
- Gupta, A., Maccario, H., Kriplani, N., and Leslie, N.R. (2016). In Cell and In Vitro Assays to Measure PTEN Ubiquitination. *Methods in molecular biology* 1388, 155-165.
- Hedrich, K., Kann, M., Lanthaler, A.J., Dalski, A., Eskelson, C., Landt, F., Schwinger, E., Vieregge, P., Lang, A.E., Breakefield, X.O., *et al.* (2001). The importance of gene dosage studies: mutational analysis of the parkin gene in early-onset parkinsonism. *Human molecular genetics* 10, 1649-1656.
- Ismail, A., Ning, K., Al-Hayani, A., Sharrack, B., and Azzouz, M. (2012). PTEN: A molecular target for neurodegenerative disorders. *Transl Neurosci* 3, 132-142.
- Itier, J.M., Ibanez, P., Mena, M.A., Abbas, N., Cohen-Salmon, C., Bohme, G.A., Laville, M., Pratt, J., Corti, O., Pradier, L., *et al.* (2003). Parkin gene inactivation alters behaviour and dopamine neurotransmission in the mouse. *Human molecular genetics* 12, 2277-2291.
- Kim, S., Domon-Dell, C., Kang, J.H., Chung, D.H., Freund, J.N., and Evers, B.M. (2004). Down-regulation of the tumor suppressor PTEN by the tumor necrosis factor- α /nuclear factor- κ B (NF- κ B)-inducing kinase/NF- κ B pathway is linked to a default I κ B- α autoregulatory loop. *Journal of Biological Chemistry* 279, 4285-4291.
- Kitada, T., Asakawa, S., Hattori, N., Matsumine, H., Yamamura, Y., Minoshima, S., Yokochi, M., Mizuno, Y., and Shimizu, N. (1998). Mutations in the parkin gene cause autosomal recessive juvenile parkinsonism. *Nature* 392, 605-608.
- Kovacs, I., and Lindermayr, C. (2013). Nitric oxide-based protein modification: formation and site-specificity of protein S-nitrosylation. *Frontiers in plant science* 4, 137.
- Kwak, Y.D., Ma, T., Diao, S., Zhang, X., Chen, Y., Hsu, J., Lipton, S.A., Masliah, E., Xu, H., and Liao, F.F. (2010). NO signaling and S-nitrosylation regulate PTEN inhibition in neurodegeneration. *Molecular neurodegeneration* 5, 49.
- Lee, C., Kim, J.S., and Waldman, T. (2004). PTEN gene targeting reveals a radiation-induced size checkpoint in human cancer cells. *Cancer research* 64, 6906-6914.
- Leonard, M.O., Cottell, D.C., Godson, C., Brady, H.R., and Taylor, C.T. (2003). The role of HIF-1 α in transcriptional regulation of the proximal tubular epithelial cell response to hypoxia. *Journal of Biological Chemistry* 278, 40296-40304.
- Lin, D.C., Xu, L., Chen, Y., Yan, H., Hazawa, M., Doan, N., Said, J.W., Ding, L.W., Liu, L.Z., Yang, H., *et al.* (2015). Genomic and Functional Analysis of the E3 Ligase PARK2 in Glioma. *Cancer research* 75, 1815-1827.

Lucking, C.B., Durr, A., Bonifati, V., Vaughan, J., De Michele, G., Gasser, T., Harhangi, B.S., Meo, G., Deneffe, P., Wood, N.W., *et al.* (2000). Association between early-onset Parkinson's disease and mutations in the parkin gene. *The New England journal of medicine* *342*, 1560-1567.

Manning, B.D., and Cantley, L.C. (2007). AKT/PKB signaling: navigating downstream. *Cell* *129*, 1261-1274.

Manzanillo, P.S., Ayres, J.S., Watson, R.O., Collins, A.C., Souza, G., Rae, C.S., Schneider, D.S., Nakamura, K., Shiloh, M.U., and Cox, J.S. (2013). The ubiquitin ligase parkin mediates resistance to intracellular pathogens. *Nature* *501*, 512-516.

Mira, M.T., Alcais, A., Nguyen, V.T., Moraes, M.O., Di Flumeri, C., Vu, H.T., Mai, C.P., Nguyen, T.H., Nguyen, N.B., Pham, X.K., *et al.* (2004). Susceptibility to leprosy is associated with PARK2 and PACRG. *Nature* *427*, 636-640.

Mookherjee, P., Quintanilla, R., Roh, M.S., Zmijewska, A.A., Jope, R.S., and Johnson, G.V. (2007). Mitochondrial-targeted active Akt protects SH-SY5Y neuroblastoma cells from staurosporine-induced apoptotic cell death. *Journal of cellular biochemistry* *102*, 196-210.

Numajiri, N., Takasawa, K., Nishiya, T., Tanaka, H., Ohno, K., Hayakawa, W., Asada, M., Matsuda, H., Azumi, K., Kamata, H., *et al.* (2011). On-off system for PI3-kinase-Akt signaling through S-nitrosylation of phosphatase with sequence homology to tensin (PTEN). *Proceedings of the National Academy of Sciences of the United States of America* *108*, 10349-10354.

Ocana, A., Vera-Badillo, F., Al-Mubarak, M., Templeton, A.J., Corrales-Sanchez, V., Diez-Gonzalez, L., Cuenca-Lopez, M.D., Seruga, B., Pandiella, A., and Amir, E. (2014). Activation of the PI3K/mTOR/AKT pathway and survival in solid tumors: systematic review and meta-analysis. *PloS one* *9*, e95219.

Ong, E.L., Goldacre, R., and Goldacre, M. (2014). Differential risks of cancer types in people with Parkinson's disease: a national record-linkage study. *European journal of cancer* *50*, 2456-2462.

Periquet, M., Latouche, M., Lohmann, E., Rawal, N., De Michele, G., Ricard, S., Teive, H., Fraix, V., Vidailhet, M., Nicholl, D., *et al.* (2003). Parkin mutations are frequent in patients with isolated early-onset parkinsonism. *Brain : a journal of neurology* *126*, 1271-1278.

Picchio, M.C., Martin, E.S., Cesari, R., Calin, G.A., Yendamuri, S., Kuroki, T., Pentimalli, F., Sarti, M., Yoder, K., Kaiser, L.R., *et al.* (2004). Alterations of the tumor suppressor gene Parkin in non-small cell lung cancer. *Clinical cancer research : an official journal of the American Association for Cancer Research* *10*, 2720-2724.

Podsypanina, K., Ellenson, L.H., Nemes, A., Gu, J., Tamura, M., Yamada, K.M., Cordon-Cardo, C., Catoretti, G., Fisher, P.E., and Parsons, R. (1999). Mutation of Pten/Mmac1 in mice causes neoplasia in multiple organ systems. *Proceedings of the National Academy of Sciences of the United States of America* *96*, 1563-1568.

Poulogiannis, G., McIntyre, R.E., Dimitriadi, M., Apps, J.R., Wilson, C.H., Ichimura, K., Luo, F., Cantley, L.C., Wyllie, A.H., Adams, D.J., *et al.* (2010). PARK2 deletions occur frequently in sporadic colorectal cancer and accelerate adenoma development

in Apc mutant mice. *Proceedings of the National Academy of Sciences of the United States of America* *107*, 15145-15150.

Saal, L.H., Gruvberger-Saal, S.K., Persson, C., Loevgren, K., Jumppanen, M., Staaf, J., Jonsson, G., Pires, M.M., Maurer, M., Holm, K., *et al.* (2008). Recurrent gross mutations of the PTEN tumor suppressor gene in breast cancers with deficient DSB repair. *Nature genetics* *40*, 102-107.

Schulz, E., Schuhmacher, S., and Munzel, T. (2009). When metabolism rules perfusion: AMPK-mediated endothelial nitric oxide synthase activation. *Circulation research* *104*, 422-424.

Siddiqui, A., Bhaumik, D., Chinta, S.J., Rane, A., Rajagopalan, S., Lieu, C.A., Lithgow, G.J., and Andersen, J.K. (2015). Mitochondrial Quality Control via the PGC1alpha-TFEB Signaling Pathway Is Compromised by Parkin Q311X Mutation But Independently Restored by Rapamycin. *The Journal of neuroscience : the official journal of the Society for Neuroscience* *35*, 12833-12844.

Song, M.S., Carracedo, A., Salmena, L., Song, S.J., Egia, A., Malumbres, M., and Pandolfi, P.P. (2011). Nuclear PTEN Regulates the APC-CDH1 Tumor-Suppressive Complex in a Phosphatase-Independent Manner. *Cell* *144*, 187-199.

Song, M.S., Salmena, L., and Pandolfi, P.P. (2012). The functions and regulation of the PTEN tumour suppressor. *Nature reviews. Molecular cell biology* *13*, 283-296.

Stevens, D.A., Lee, Y., Kang, H.C., Lee, B.D., Lee, Y.I., Bower, A., Jiang, H., Kang, S.U., Andrabi, S.A., Dawson, V.L., *et al.* (2015). Parkin loss leads to PARIS-dependent declines in mitochondrial mass and respiration. *Proceedings of the National Academy of Sciences of the United States of America* *112*, 11696-11701.

Szasz, A.M., Lanczky, A., Nagy, A., Forster, S., Hark, K., Green, J.E., Boussioutas, A., Busuttill, R., Szabo, A., and Gyorffy, B. (2016). Cross-validation of survival associated biomarkers in gastric cancer using transcriptomic data of 1,065 patients. *Oncotarget* *7*, 49322-49333.

Tay, S.P., Yeo, C.W., Chai, C., Chua, P.J., Tan, H.M., Ang, A.X., Yip, D.L., Sung, J.X., Tan, P.H., Bay, B.H., *et al.* (2010). Parkin enhances the expression of cyclin-dependent kinase 6 and negatively regulates the proliferation of breast cancer cells. *The Journal of biological chemistry* *285*, 29231-29238.

Trachootham, D., Lu, W., Ogasawara, M.A., Nilsa, R.D., and Huang, P. (2008). Redox regulation of cell survival. *Antioxidants & redox signaling* *10*, 1343-1374.

Trotman, L.C., Niki, M., Dotan, Z.A., Koutcher, J.A., Di Cristofano, A., Xiao, A., Khoo, A.S., Roy-Burman, P., Greenberg, N.M., Van Dyke, T., *et al.* (2003). Pten dose dictates cancer progression in the prostate. *PLoS biology* *1*, E59.

Unoki, M., and Nakamura, Y. (2001). Growth-suppressive effects of BPOZ and EGR2, two genes involved in the PTEN signaling pathway. *Oncogene* *20*, 4457-4465.

Veeriah, S., Taylor, B.S., Meng, S., Fang, F., Yilmaz, E., Vivanco, I., Janakiraman, M., Schultz, N., Hanrahan, A.J., Pao, W., *et al.* (2010). Somatic mutations of the Parkinson's disease-associated gene PARK2 in glioblastoma and other human malignancies. *Nature genetics* *42*, 77-82.

Wang, F., Denison, S., Lai, J.P., Philips, L.A., Montoya, D., Kock, N., Schule, B., Klein, C., Shridhar, V., Roberts, L.R., *et al.* (2004). Parkin gene alterations in hepatocellular carcinoma. *Genes, chromosomes & cancer* 40, 85-96.

Wongseree, W., Assawamakin, A., Piroonratana, T., Sinsomros, S., Limwongse, C., and Chaiyaratana, N. (2009). Detecting purely epistatic multi-locus interactions by an omnibus permutation test on ensembles of two-locus analyses. *BMC bioinformatics* 10, 294.

Xiao, B., Sanders, M.J., Carmena, D., Bright, N.J., Haire, L.F., Underwood, E., Patel, B.R., Heath, R.B., Walker, P.A., Hallen, S., *et al.* (2013). Structural basis of AMPK regulation by small molecule activators. *Nat Commun* 4.

Yeo, C.W., Ng, F.S., Chai, C., Tan, J.M., Koh, G.R., Chong, Y.K., Koh, L.W., Foong, C.S., Sandanaraj, E., Holbrook, J.D., *et al.* (2012). Parkin pathway activation mitigates glioma cell proliferation and predicts patient survival. *Cancer research* 72, 2543-2553.

Yuan, M., Breitkopf, S.B., Yang, X., and Asara, J.M. (2012). A positive/negative ion-switching, targeted mass spectrometry-based metabolomics platform for bodily fluids, cells, and fresh and fixed tissue. *Nature protocols* 7, 872-881.

Yuan, T.L., and Cantley, L.C. (2008). PI3K pathway alterations in cancer: variations on a theme. *Oncogene* 27, 5497-5510.

Zhang, C., Lin, M., Wu, R., Wang, X., Yang, B., Levine, A.J., Hu, W., and Feng, Z. (2011). Parkin, a p53 target gene, mediates the role of p53 in glucose metabolism and the Warburg effect. *Proceedings of the National Academy of Sciences of the United States of America* 108, 16259-16264.

FIGURE LEGENDS

Figure 1. Genetic landscape of *PARK2* copy-number and mRNA expression across human cancers.

(A) Frequencies of *PARK2* deletion from 9,863 primary tumors across 28 different cancer types. Colored bars describe the percentage of tumor samples showing focal deletion; dark blue, overall deletion; light blue, diploid/no focal gain; grey.

(B) Frequencies of relative fold-change of *PARK2* mRNA underexpression between cancerous and corresponding normal tissues (≥ 0.5 and ≥ 1 -log₂-fold change in tumor versus normal). The analysis was performed on 13,481 specimens from 25 different cancer types (mRNA downregulated ≥ 1 -log₂-fold change; red, mRNA downregulated ≥ 0.5 -log₂-fold; yellow, no loss of mRNA expression; grey). The putative DCN and mRNA expression data for *PARK2* were retrieved from the TCGA database.

(C) *PARK2* mRNA expression in subgroups of primary GBMs of different ploidy status, ranging from gain (N=24), to diploid (N=376), heterozygous deletion; Hetloss (N=158) and homozygous deletion; Homdel (N=19) ($P = 3.5 \times 10^{-7}$, one-way Anova analysis).

(D) Representative IHC staining intensities of PARKIN protein expression across 61 GBM specimens.

(E) Kaplan-meier survival plots of glioma cancer patients stratified by tumors bearing *PARK2* deletion versus retention [left; *PARK2* Deleted: ≤ 1.8 copies (n=24), *PARK2* Diploid: = 2 copies, (n=149)], low versus intermediate *PARK2* mRNA expression [middle; *PARK2* Low: ≥ 2 x lower than log₂ median expression (n=92), *PARK2* Intermediate: < 2 x lower or higher than log₂ median expression (n=251)], and positive versus negative IHC PARKIN protein expression (right) (from left to right: $P = 0.032$, $P = 4 \times 10^{-4}$, $P = 0.01$, Log-rank test).

See also **Figure S1** and **Tables S1-2**.

Figure 2. *PARK2* depletion contributes to the activation of the PI3K/Akt pathway.

(A) Immunoblotting analysis of HCT116 cells stably transfected with control *GFP* (shGFP) or *PARK2* (shPARK2_1 and shPARK2_2) lentiviral hairpins.

(B) MTS assay and (C) Caspase 3/7 activity assay of shGFP or shPARK2 HCT116 cells, following treatment with increasing concentrations of staurosporine (50nM and 100nM) for 1 hour (MTS assay; $P = 0.001$ for 50nM, and $P = 0.0008$ for 100nM treatment, caspase 3/7 assay; $P = 0.043$ for 50nM, $P = 0.036$ for 100nM treatment).

(D) Immunoblotting analysis of shGFP and shPARK2 HCT116 cells following treatment with the indicated compounds; 1 μ M BKM (NVP-BKM120) or 500 nM BEZ (NVP-BEZ235) for 24 hours, 500 nM MK (MK 2206) for 4 hours, 100nM Rapa (Rapamycin) or Torin for 2 hours, 100 nM PD0 (PD0325901) for 1 hour or 10 nM GSK (GSK1120212) for 6 hours.

(E) Drug dose-response curves of shGFP and shPARK2 HCT116 cells treated with the indicated compounds for 24 hours (NVP-BKM120; $P = 0.014$, NVP-BEZ235; $P = 9.28 \times 10^{-5}$, MK 2206; $P = 1 \times 10^{-4}$, Rapamycin; $P = 1.45 \times 10^{-11}$, Torin; $P = 6.73 \times 10^{-10}$, PD0325901; $P = 0.02$, GSK1120212; $P = 0.03$, two-way Anova analysis). Data are represented as mean \pm SEM (* $P < 0.05$, ** $P < 0.01$, 2-tailed *t* test).

See also **Figure S2**.

Figure 3. *PARK2* overexpression suppresses Akt activation, and mitigates cell proliferation and migration in *PTEN* wild-type, but not *PTEN* mutant cells.

Immunoblotting analysis of

(A) HCT116 cells transfected with vector only or vector encoding WT *PARK2*.

(B) *PTEN* WT H1299 cells and

(C) *PTEN* mutant PC3 cells expressing vector only or vector encoding WT *PARK2* following 10% FBS stimulation. Cells were serum-starved for 24 hours prior to FBS stimulation.

(D) Cell proliferation (HCT116 *PTEN*^{+/+}; $P = 0.002$, HCT116 *PTEN*^{-/-}; $P = 0.99$, H1299; $P = 3.4 \times 10^{-5}$, PC3; $P = 0.66$, two-way Anova analysis) and

(E) Cell migration assays of *PTEN*-WT (HCT116 *PTEN*^{+/+} and H1299) and *PTEN*-deficient (HCT116 *PTEN*^{-/-} and PC3) cells expressing vector only or vector encoding WT *PARK2* (HCT116 *PTEN*^{+/+}; $P = 8.1 \times 10^{-4}$, HCT116 *PTEN*^{-/-}; $P = 0.99$, H1299; $P = 4.7 \times 10^{-3}$, PC3; $P = 0.68$).

(F) BLI images of NOD/SCID mice retro-orbitally injected with luciferase labelled H1299 cells expressing EV or human *PARK2*. Images were taken at 3 and 4 weeks post-injection (W3 and W4) to assess for luciferase-expressing lung metastases.

(G) Quantification of BLI intensities on week 3 and 4 post-injection (EV; $P = 0.02$ and human *PARK2*; $P = 0.54$). The lungs were then dissected from the mice for H&E staining.

(H) Scatterplot indicating that overexpression of *PARK2* significantly mitigated the formation of lung metastases in NOD/SCID mice ($P = 0.006$).

(I) Representative H&E staining of lung sections 4 weeks post-injection to highlight significantly more and larger size metastatic tumor lesions in the mice injected with vector only or with vector encoding WT *PARK2* H1299 cells. Data are represented as mean \pm SEM (n.s.: not significant, * $P < 0.05$, ** $P < 0.01$, 2-tailed t test).

See also **Figure S2**.

Figure 4. *PARK2* depletion contributes to Akt activation in a *PTEN*-dependent manner.

(A-B) Immunoblotting of shGFP and shPARK2 *PTEN* WT HCT116^{parental}, H460 and HCT116^{PTEN+/+} or *PTEN* mutant PC3, U138 and HCT116^{PTEN-/-} cells.

(C) Quantitative real-time PCR for *PARK2* and *PTEN* on mRNA isolated from shGFP and shPARK2 HCT116 cells (*PARK2* qPCR; $P = 0.001$, *PTEN* qPCR; $P = 0.44$).

(D) *PTEN* activity assay ($P = 0.015$), and

(E) Phosphoinositide PI(3,4,5)P₃ and PI(3,4)P₂ levels between shGFP and shPARK2 HCT116 cells [PI(3,4,5)P₃; $P = 0.002$, PI(3,4)P₂; $P = 0.015$]. *PTEN* was ectopically expressed equally between cells.

(F) Immunoblotting of shGFP and shPARK2 HCT116 cells with or without treatment with 10 μ M MG132 for 6 hours. Data are represented as mean \pm SEM (n.s.: not significant, * $P < 0.05$, ** $P < 0.01$, 2-tailed t test).

See also **Figures S3** and **S4**.

Figure 5. The role of *PARK2* depletion in cellular metabolism and AMPK-mediated eNOS activation.

(A) Seahorse analysis of OCR following sequential injection of oligomycin, FCCP and antimycin A/rotenone (n=6),

(B) OCR of basal ($P = 0.016$), maximal ($P = 0.003$) and non-mitochondrial respiration ($P = 0.037$),

(C) Relative ATP levels ($P = 0.02$), and

(D) Immunoblotting analysis between shGFP and shPARK2 HCT116 cells.

(E) Schematic representation of NO biosynthesis involving the conversion of L-arginine into L-citrulline by NOS in the presence of cofactors including NADPH, FAD, FMN, CaM, O₂ and BH₄.

(F) Relative abundance of metabolites involved in NO biosynthesis following *PARK2* knockdown in HCT116 cells (FAD; $P = 0.002$, FMN; $P = 0.011$, NADP; $P = 0.025$, NADPH; $P = 0.019$, Arginine; $P = 0.063$, Citrulline, $P = 0.24$).

(G) Relative NOS activity ($P = 0.017$),

(H) Oxidised NO levels ($P = 5.1 \times 10^{-4}$),

(I) NADP/NADPH levels ($P = 0.013$),

(J) ROS levels following 2 hours menadione treatment (20uM) ($P = 0.006$),

(K) GSH/GSSG levels between shGFP and shPARK2 HCT116 cells ($P = 0.008$).

Immunoblotting analysis of

(L) shGFP and shPARK2 HCT116 cells with or without treatment with 5mM GSH-MEE for 72 hours.

(M) HCT116 cells following treatment with the indicated concentrations (0-20 μ M) of the allosteric AMPK activator 991 for 5 hours. Cells were serum-starved for 2 hours prior to 991 treatment. Data are represented as mean \pm SEM (n.s.: not significant, * $P < 0.05$, ** $P < 0.01$, 2-tailed t test).

See also **Figure S4**.

Figure 6. *PARK2* depletion leads to enhanced S-nitrosylation and ubiquitination of PTEN.

(A) Anti-PTEN immunoprecipitates (IP) derived from MYC-tagged transfected *PTEN* HCT116 cells expressing *GFP* or *PARK2* shRNA.

(B) Fluorometric measurement of S-nitrosylated PTEN between shGFP and shPARK2 HCT116 cells. SNO-PTEN was assessed by NO release, causing the conversion of DAN to the fluorescent compound NAT ($P = 0.009$).

(C) Immunoblotting analysis of whole-cell lysates and

(D) Anti-PTEN immunoprecipitates (IP) derived from HA-ubiquitin (Ub) and Myc-tagged *PTEN* transfected HCT116 cells expressing *GFP* or *PARK2* shRNA. Where indicated cells were treated with MG132 (10 μ M) for 6 hours before collection.

Immunoblotting analysis and anti-PTEN immunoprecipitates derived from

(E) Myc-tagged WT or C83S mutant *PTEN*-transfected HCT116 cells expressing *GFP* or *PARK2* shRNA.

(F) WT *PTEN*-transfected shGFP and shPARK2 HCT116 cells, 48 hours post-transfection with scrambled or AMPK α 1 and AMPK α 2 siRNAs.

(G) Parental HCT116 treated (or not treated) with the allosteric AMPK activator 991 for 5 hours (20 μ M) following 2 hours serum starvation (left), or with 25mM glucose-containing DMEM (middle) for 6 hours, or with oligomycin (5 μ M) for 2 hours. Data are represented as mean \pm SEM.

See also **Figures S5** and **S6**.

Figure 7. *In vivo* role of *Park2* depletion in *Pten* heterozygous knock-out mice

(A) Types and frequencies of hamartomas/adenomas/carcinomas/other neoplasms found in *Pten*^{+/-} mice with WT, HET or HOM deletion of *Park2*.

(B) Frequencies of low- and high-grade prostatic intraepithelial neoplasia (PIN) lesions, prostatic low-grade adenocarcinoma and

(C) Different stages of thyroid adenoma/carcinoma lesions found in *Pten*^{+/-} mice in the presence/absence of monoallelic or biallelic *Park2* deletion (Prostate lesions: $P = 9.3 \times 10^{-12}$, Thyroid lesions: $P = 0.002$, Chi-squared test).

(D) Representative H&E-stained sections of the low- (left) and high-grade (middle) PIN lesions and low-grade adenocarcinoma (right) found in *Pten*^{+/-} mice with or without *Park2* deletion. Scale bar is 250-500 μm .

(E) Kaplan–Meier survival plot of *Pten*^{+/-} mice bearing WT (red) (n=21) or HET (blue) (n=27) *Park2* deletion ($P = 0.0108$, Log-rank test).

(F) Kaplan–Meier survival plot of *Pten*^{+/-} mice bearing WT (red) (n=21) or HOM (green) (n=24) *Park2* deletion. Both HET and HOM deletion of the *Park2* gene significantly increased the cancer-related mortality of *Pten*^{+/-} mice ($P = 0.0015$, Log-rank test).

See also **Figure S7**.

Contact for Reagents and Resource Sharing

Further information and requests for resources and reagents should be directed to and will be fulfilled by the Lead Contact, George Poulgiannis (George.Poulgiannis@icr.ac.uk).

Experimental Model and Subject Details

Mice

Pten^{+/-} heterozygous mice (Di Cristofano et al., 1998) were bred with mice harbouring a targeted knockout of *Park2* exon 3 (Itier et al., 2003). All mice were previously backcrossed over ten generations and maintained in a C57BL/6 background and they were genotyped by PCR for *Pten* and *Park2* alleles as described previously (Di Cristofano et al., 1998; Itier et al., 2003). Tumor-bearing mice were euthanized and subjected to whole-body histological analysis. Normal and tumor tissues were fixed in 4% PFA, embedded in paraffin, sectioned, and subjected to hematoxylin and eosin (H&E) staining for pathological evaluation. Survival analyses were performed using Kaplan–Meier curves and the Log-rank test. Six- to eight-week old NOD.CB17-Prkdc^{scid}/J mice were injected via the retrobulbar sinus with 200 µl cell suspension (1x10⁶ cells) of GFP flow-sorted luciferase labeled (pLV430G-oFL-T2A-eGFP) H1299 cells expressing pLenti6UbCV5-DEST- empty vector or *PARK2*. Development of metastases was monitored by luciferin injection and bioluminescence imaging at 3 and 4 weeks post-injection. Bioluminescence (BLI) signal intensities were determined by using the region of interest (ROI) tool in Living Image® Software (PerkinElmer). After the last imaging session the mice were euthanized and the lungs were surgically removed and inflated with 4% formalin in PBS. Lung sections, 5 µm, were subjected to H&E staining and the number of lung tumor nodules was counted using a dissection microscope. All mice were maintained according to NIH-approved institutional animal care guidelines and the study was approved by the Institutional Committee at the Beth-Israel Deaconess Medical Center.

Cell Culture

293T and PC3 cells were cultured in DMEM supplemented with 10% fetal bovine serum (FBS), 100 U/ml penicillin and 100 µg/ml streptomycin. HCT116 parental and isogenic PTEN null cell lines (Lee et al., 2004) were cultured in McCoy's 5A, H460 and H1299 cells in RPMI, and U138 cells in DMEM-F12, all supplemented as above. The breast cancer cell lines MDA-MB-134, BT-474, UACC-812, MCF-7, Hs-578T, SK-BR-3, AU-565, BT-20 and JIMT-1 were cultured in DMEM, and the ZR-75-30 cells in RPMI, all supplemented as above. MCF10A parental and isogenic PTEN null cells were cultured in DMEM supplemented with 5% horse serum (HS) (ThermoFisher, 16050-122), 20 ng/ml EGF (PeproTech, AF-100-15), 0.5 mg/ml hydrocortisone (Sigma-Aldrich, H0888), 100 ng/ml cholera toxin (Sigma-Aldrich, C8052), 10 µg/ml insulin (Sigma-Aldrich, I1882), supplemented with penicillin and streptomycin as above. All cell lines were maintained at 37°C in a humidified incubator with 5% CO₂ and were tested and confirmed to be negative for mycoplasma infection. For glucose starvation experiments, cells were washed twice with PBS and then incubated in DMEM without glucose and sodium

pyruvate supplemented with 10% dialyzed FBS for 6 hours. For treatment with the allosteric AMPK activator 991 (Xiao et al., 2013), cells were serum-starved for 2 hours prior to 991 treatment for 5 hours. All cell lines used in the study were submitted to Eurofins Genomics for autosomal short tandem repeat (STR) authentication.

Method details

Transfections

For lentiviral gene knockdown, pLKO.1 shRNA sequences against human *PARK2* or *GFP* control were transfected in 293T cells using the FuGENE 6 transfection reagent (Promega, E2691) according to the manufacturer's protocols. Infected cells were selected in the presence of 2 µg/ml puromycin (InvivoGen, ant-pr-5b) for at least 4 days. Stably expressing cancer cell lines were established by infecting with virus encoding human wild-type *PARK2*, the E3 ligase dead C431S mutant or empty vector in the pLenti6UbCV5-DEST backbone (ThermoFisher, V49910). Infected cells were selected in the presence of 2-10 µg/ml blasticidin (InvivoGen, ant-bl-1) for 2 weeks. For stable expression of luciferase and GFP, H1299 cells were infected with pLV430G-oFL-T2A-eGFP (Green et al., 2015), a lentivirus expressing the luciferase gene cloned in a eGFP expressing vector (gift from Dr Tina Yuan, Dana-Farber Cancer Institute, Harvard Medical School, Boston), and GFP-positive cells were sorted by flow cytometry 1 week after infection. H460 cells were transfected with *PARK2* sgRNA CRISPR/Cas9 All-in-One Lentivector Target 3 (Applied Biological Materials, K1594608) or control LentiCRISPR v2 according to the manufacturer's instructions. Infected cells were selected in the presence of 2 µg/ml puromycin for 4 days and isolation of *PARK2* clonal deletion mutants was validated by immunoblotting analysis and DNA sequencing.

Immunoblot Analysis

Cells were washed with ice-cold PBS and lysed on ice for 30 min with cell lysis buffer containing 20 mM Tris-HCl (pH 7.5), 150 mM NaCl, 1 mM EDTA, 1 mM EGTA, 1% Triton X-100, supplemented freshly with a protease and phosphatase inhibitor cocktail (5872, Cell Signaling Technology), 10nM Calyculin A (Cell Signaling Technology, 9902) and 1 mM DTT (ThermoFisher, R0861). Lysates were subjected to centrifugation at 12,000g for 10 min at 4°C and protein concentrations were determined using the Bradford assay (Bio-Rad, 5000006). Protein lysates were boiled for 10 min and subjected to SDS-PAGE electrophoresis. Densitometry was calculated using the Image Lab Software 5.2.1 (Bio-Rad).

Immunohistochemistry

The GBM tissue microarray (TMA) was prepared and characterized as described previously from the Tumor Tissue Bank at University Health Network, University of Toronto (Agnihotri et al., 2012). Briefly, the TMA was de-waxed in xylene followed by rehydration in a standard alcohol series. Antigen retrieval was by pressure cooking for 20 min in citrate buffer (pH 6.0), followed by blocking of endogenous peroxidase in 0.3% H₂O₂. Antibody incubation was

performed using the ABC reagent kit (Vector Labs, PK-6100) as per manufacturers instructions. Briefly, Parkin antibody (ThermoFisher, PA1-38412) was diluted 1:100 in antibody diluent and added to the slides and incubated overnight at 4°C. Detection was performed using biotinylated secondary antibodies for 30 min, the ABC reagent kit and 3,3'-Diaminobenzidine chromogen. Sections were counter-stained with hematoxylin (ThermoFisher, 008001) for 30 secs, dehydrated in 70, 80 and 100% ethanol, briefly washed in xylene and mounted in Permount (ThermoFisher, SP-15). For PTEN and phospho-AKT immunohistochemistry of mouse tumor sections, antigen retrieval was carried out by microwave heating for 20 min in citrate buffer (pH 6.0). Anti-PTEN (Dako, M3627) and anti-phospho-Akt (Ser473) (Cell Signaling Technology, 4060) antibodies were applied at dilutions of 1:200 and 1:50 respectively. PTEN and phospho-Akt IHC staining intensity was graded as 0 (negative), 1 (weak), 2 (moderate), and 3 (strong). Images were captured on a Nikon E-600 microscope and analyzed using Nikon ACT-1 software.

PTEN phosphatase activity assay

For PTEN phosphatase activity assay, PTEN-transfected cells [pRK5-Myc-PTEN-WT, (Song et al., 2011)] were lysed in lysis buffer containing protease and phosphatase inhibitors in the absence of DTT. PTEN was immunoprecipitated from 1 mg of cell lysates and the PTEN phosphatase activity was measured using a PTEN activity ELISA kit (Echelon Biosciences Inc, K-4700), following the manufacturer's instructions. Where indicated, PTEN immunoprecipitates were treated with 50 mM DTT at 4°C for 30 min prior to measuring PTEN phosphatase activity.

Detection of S-nitrosylated PTEN

S-nitrosylation of PTEN was detected using the 2,3-diaminonaphthalene (DAN) assay. Briefly, PTEN transfected cells (pRK5-Myc-PTEN-WT) were lysed in lysis buffer containing protease and phosphatase inhibitors and 40 mM N-ethylmaleimide in the absence of DTT. PTEN was immunoprecipitated from equal volume of the diluted cell lysates containing 1 mg of soluble protein. The immunoprecipitates were washed twice with lysis buffer and twice with PBS. The pellet was resuspended in 500 µl of PBS and 100 µM HgCl₂ and 100 µM DAN was added. The samples were incubated in the dark at room temperature (RT) for 30 min and 1 M NaOH was added. The generated fluorescent triazole from the reaction of DAN with the NO released from PTEN was measured using an excitation wavelength of 375 nm and an emission wavelength of 450 nm. As a negative control, the PTEN antibody alone in lysis buffer was immunoprecipitated and the resulting background fluorescence intensity was subtracted from each sample. S-nitrosylated PTEN was confirmed by immunoblotting of immunoprecipitated PTEN with anti-S-nitrosocysteine antibody (Abcam, ab94930), under non-reducing conditions. For non-reducing SDS-PAGE, β-mercaptoethanol was omitted from the loading buffer and samples were not boiled.

In cell PTEN ubiquitination assay

Cellular assays to measure PTEN polyubiquitination were performed as described previously (Gupta et al., 2016). Briefly, cells were transfected with vectors encoding wild-type *PTEN* in the pRK5-Myc vector and HA-Ub and lysed in the presence of 40 NEM and supplemented freshly with a protease and phosphatase inhibitor cocktail. Equal volume of the diluted cell lysates containing 1mg of soluble protein was incubated with 1 µg mouse monoclonal anti-PTEN (Santa Cruz Biotechnology, sc-7974) or 2 µg mouse anti-HA (BioLegend, 901501) antibodies pre-coupled with protein G sepharose beads (Sigma-Aldrich, P3296) and incubated at RT for 2 hours rotating. Beads were washed four times in immunoprecipitation buffer (50 mmol/L Tris, pH 7.6, 100 mmol/L NaCl, 2 mmol/L EDTA, and 0.2% Nonidet P-40) and the bound proteins were released by boiling in SDS-PAGE sample buffer for 10 min, prior to SDS-PAGE analysis and immunoblotting with the indicated antibodies.

³H-labeling of phosphoinositides and HPLC analysis

Subconfluent cells in 10-cm dishes were labeled in 8 ml of inositol-free DMEM and 10% dialyzed FBS supplemented with 160 µCi ³H-myo-inositol (PerkinElmer, NET1168001MC, specific activity = 20.1 Ci/mmol) for 24 hours. Deacylated phosphoinositides were resolved by HPLC using an Agilent 1200 Quaternary system, and radioactivity detected in-line using a Packard Flo-one Radiomatic detector. HPLC Buffer A is 1 mM EDTA, and Buffer B is 1 mM EDTA and 1 M NaH₂PO₄. An Agilent Zorbax SAX column (5 µm, 4.6 X 250 mm) was eluted by gradient program (from 100% A to 2% B at 1 min, 14% B at 30 min, 30% B at 31 min, 66% at 60 min, 100% B at 85 min, 100% A at 86 min, and hold at 100% A until 110 min) at a flow rate of 1 ml/min. PI(3,4)P₂, PI(3,4,5)P₃ standards were prepared by reacting PI3K with PI4P and PI5P, respectively and [γ -³²P]ATP.

MTS and caspase-3/7 assays

Cell viability was assessed using the CellTiter96® AQueous non-radioactive cell proliferation assay [3-(4,5-dimethylthiazol-2-yl)-5-(3-carboxymethoxyphenyl)-2-(4-sulfophenyl)-2H-tetrazolium, inner salt; MTS] (Promega, G5421) according to the manufacturer's protocol. Caspase-3/7 activities were measured using the Caspase-Glo® 3/7 assay (Promega, G8090) following treatment with 50 or 100 nM staurosporine (Sigma-Aldrich, S4400) for 1 hour. For both cell viability and caspase 3/7 assays, HCT116 cells were seeded at 3x10⁴ cells/well in a 96-well plate and incubated overnight before treatment.

Cell proliferation and cell migration assays

Proliferation kinetics of H1299, PC3, HCT116 *PTEN*^{+/+} and HCT116 *PTEN*^{-/-} cells transfected with pLenti6/UbC/V5-DEST-PARK2-WT, PARK2-C431S mutant or empty vector were determined using the Sulforhodamine B (SRB) (Sigma-Aldrich, S1402) assay over a period of 5 days. The same method was applied for shGFP and shPARK2-expressing PC3 cells transfected with pHR-SIN-PTEN-WT, PTEN-C83S and control empty vector. Briefly, 2x10³

cells were seeded in a 96-well plate in triplicate and allowed to adhere for 24 hours (Day 0). Cells were fixed at days 0, 1, 3 and 5 as follows: they were fixed with 10% trichloroacetic acid at 4°C for 60 min and washed 4x with 100 µl dH₂O. After being left to dry at RT, the cells were stained for 10 min with 0.4% (w/v) SRB dissolved in 1% acetic acid, and protein-bound dye was extracted with 10 mM unbuffered Tris base pH 10.5. Absorbance was determined at 510 nm using a 96-well microplate reader and data presented indicate the average number of triplicate experiments ± standard error of the mean (SEM).

For cell migration assays, cells were starved overnight in 0.5% FBS and 5x10⁴ cells/well were seeded in 24-well transwell chambers (Corning, Lowell, MA, USA; 8 mm pore size) in a total volume of 300 µl 0.5% FBS-media. 750 µl of media (supplemented with 10%FBS) were added to the bottom of the transwells and the plates were returned to 37°C for 24-hour incubation. The transwell inserts were washed twice in PBS and cells were fixed in 10% trichloroacetic acid (TCA) for 1 hour. The TCA containing media was removed and the inserts were washed 3x in H₂O. Cells were stained in 0.4% (w/v) SRB dissolved in 1% acetic acid for 10 min. The inserts were washed 3x in 1% acetic acid and the cells on the top of the filter were removed using a cotton swab. Migrated SRB-stained cells in the bottom of the transwell inserts were counted under a light microscope at 20x magnification in 5 fields/well.

Cytotoxicity and clonogenic assays

For determination of the IC₅₀ values of 2-DG and DCA, shGFP- or shPARK2-expressing PC3 cells were co-transfected with pHR-SIN-PTEN-WT, PTEN-C83S and control empty vector. 48 hours post transfection, the cells were seeded at 5x10³ cells/well in a 96-well plate and treated with various concentrations of 2-DG (0.5-50 mM) or DCA (5-80 mM) for 72 hours followed by SRB staining. For clonogenic assays, cells were plated at 1x10² cells/well in 24-well plates and treated with 10 mM DCA or 0.5 mM 2-DG. After 10 days, colonies were stained with a Crystal Violet solution (0.5% Crystal Violet, Sigma, 30% ethanol and 3% formaldehyde) and were counted in a GelCount™ (Oxford Optronix). Every experiment was performed in triplicate and data are presented as mean values ±SEM.

Real-Time qRT-PCR

Total RNA was extracted using the ReliaPrep RNA cell miniprep system (Promega, Z6010) according to the manufacturer's instructions. Reverse transcription and real-time PCR reactions were carried out using the QuantiTect reverse transcription kit (Qiagen, 205310) and SYBR select master mix (ThermoFisher, 4472908) respectively, using the TProfessional ThermoCycler from Biometra. The data presented are the mean values obtained ±SEM from triplicate reactions. Primer sequences used are as follows; Human *PARK2*, sense: TCAATCTACAACAGCTTTTATG, anti-sense: TGCACTAGTCCCAGGGCA (Hedrich et al., 2001), Human *PTEN*, sense: CAAGATGATGTTTGAAACTATTCCAATG, anti-sense: CCTTTAGCTGGCAGACCACAA (Kim et al., 2004), Human *18S*, sense:

GTGGAGCGATTTGTCTGGTT, anti-sense: CGCTGAGCCAGTCAGTGTAG (Leonard et al., 2003).

ROS, NO, GSH/GSSG and NOS activity measurements

H₂O₂ levels were measured using the ROS-Glo™ H₂O₂ assay (Promega, G8820) according to the manufacturer's instructions. Briefly, 1x10⁴ shGFP control and shPARK2-expressing cells were seeded in a 96-well plate and incubated at 37°C and 5% CO₂ for 18 hours. Cells were washed with PBS and treated in Hank's BSS medium containing 20 µM menadione (Sigma-Aldrich, M5625) in the presence of 20 µl 125 µM H₂O₂ substrate (provided in the kit). Following incubation at 37°C for 2 hours, 100 µl of ROS-Glo detection solution was added to the wells and the plate was incubated for 20 min at RT. Luminescence was determined with a microplate reader and the average relative light units (RLU) ±SEM of triplicate data are reported.

Nitric oxide (NO) levels were detected using the Nitric Oxide Assay Kit (abcam, ab65327) according to the manufacturer's protocol. Briefly, shGFP and shPARK2-expressing cells were grown in regular culture medium for 24 hours. After washing with cold PBS, 2x10⁶ cells were resuspended in 500 µl assay buffer and homogenised quickly by pipetting up and down a few times. The samples were centrifuged for 5 min at 4°C at top speed to remove any insoluble material. Triplicate 75 µl aliquots of the supernatant were transferred to a 96-well plate and 5 µl of enzyme cofactor and 5 µl of nitrate reductase were added to each of the reaction wells. The plate was incubated at RT for 3 hours and 5 µl of enhancer was added to each well, before further incubation for 30 min at RT. 5 µl of the DAN probe was added to each well, the plate was incubated at RT for 10 min and 5 µl of NaOH was added before final incubation at RT for 10 min. Fluorescence was determined with a microplate reader at Ex/Em = 360/450nm. All reagents were provided in the kit. GSH:GSSG levels were measured using the GSH/GSSG-Glo™ Assay kit (Promega, V6611) and nitric oxide synthase (NOS) activity was determined using the NOS activity assay kit (BioVision, K205-100) according to the manufacturer's protocol.

Mitochondrial flux analysis

PARK2 and *GFP* stable knockdown cells were plated at 2x10⁴/well in a 96-well Seahorse cell culture microplate and incubated overnight. The next morning, culture media was replaced with pH-adjusted (pH=7.4±0.1) bicarbonate-free DMEM with 10 mM Glucose, 1 mM sodium pyruvate and 2 mM L-Glutamine and the plate was incubated at 37°C for 1 hour in a non-CO₂ incubator. Oxygen consumption rates were measured using the Seahorse XF Cell Mito Stress Kit (Agilent, 103015-100) on a XFe96 Analyzer. 2 µM Oligomycin, 0.5 µM FCCP, and 0.5 µM rotenone/antimycin (R/A) were used for all conditions. Cell numbers were normalised using Cyquant (ThermoFisher, C35012).

Tandem Mass Spectrometry

Metabolite levels were determined by targeted liquid-chromatography tandem mass spectrometry (LC-MS/MS) analysis as described previously (Yuan et al., 2012). Briefly, 48 hours prior to each experiment, 2.5×10^5 HCT116 cells expressing shGFP or shPARK2 were seeded in 6-cm dishes. The media for each plate was replaced 2 hours prior to metabolite extraction and after aspiration, 4 mL pre-chilled (at $-80\text{ }^{\circ}\text{C}$) methanol was added to the cells on dry ice for 15 min. Cell extracts were collected into 15 mL conical tubes and centrifuged for 5 min at 4200 rpm. Solvent in the resulting supernatant was evaporated using a centrifugal vacuum evaporator ("SpeedVac") and samples were re-suspended in 20 μL HPLC-grade water for mass spectrometry. 8 μL were injected and analyzed using a Prominence UFLC HPLC system (Shimadzu) for hydrophilic interaction liquid chromatography (HILIC), coupled to a QTRAP 5500 hybrid triple quadrupole/linear ion trap mass spectrometer (SCIEX) operated in the selected reaction monitoring (SRM) mode. Peak areas of LC-SRM-MS traces for each metabolite were integrated using the MultiQuant v1.1 software (SCIEX).

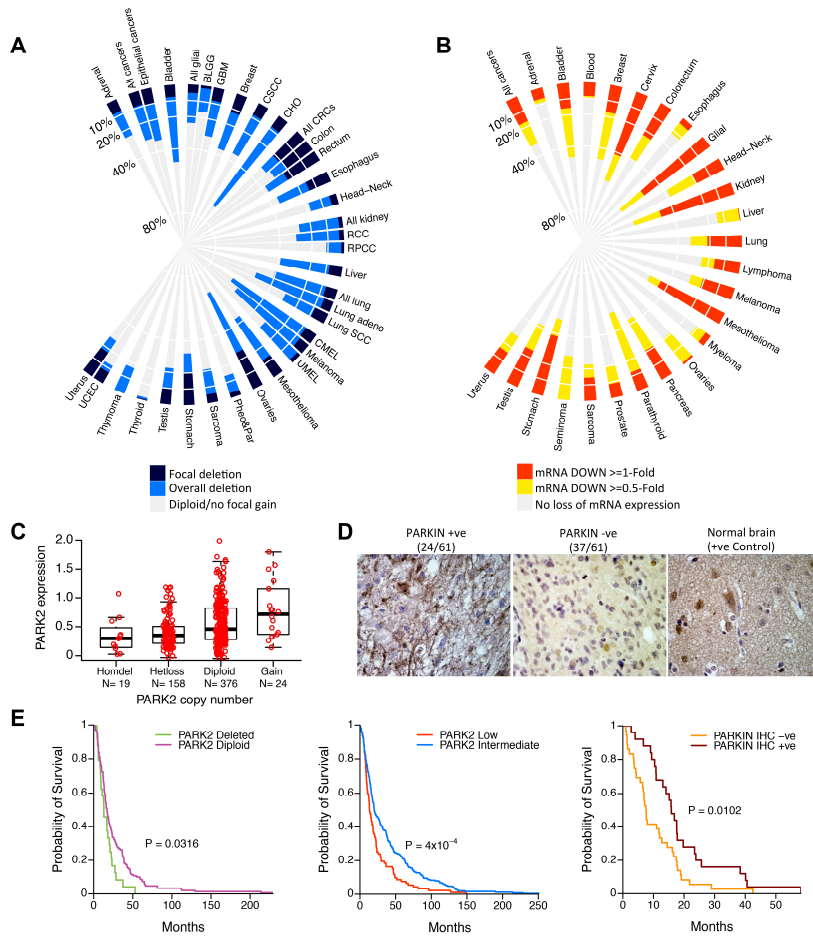
Quantification and Statistical Analysis

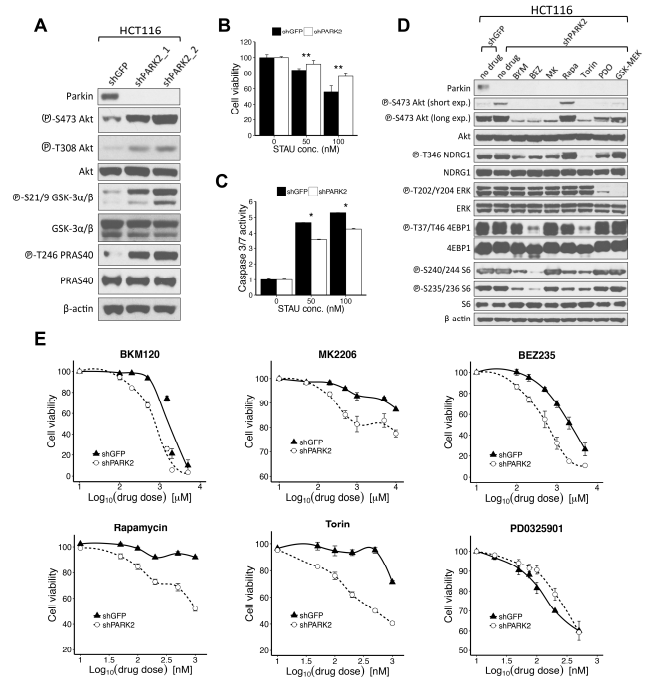
Bioinformatic Analysis

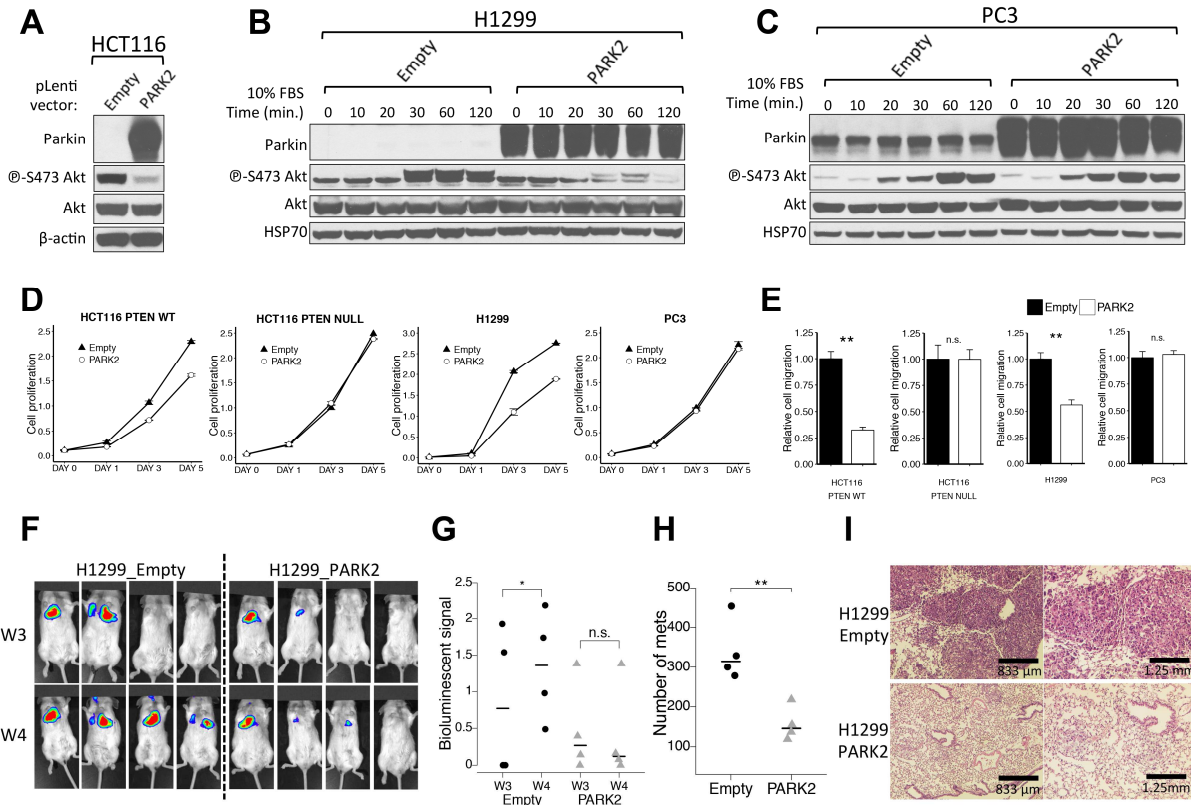
GISTIC (Genomic Identification of Significant Targets in Cancer) analyses were performed on DNA copy number data from the SNP pipeline version 3.0. 9,863 tumor samples across 28 cancer types were selected for this analysis using the 2015-06-01 stddata TCGA/GDAC tumor sample sets from FireHose, and the frequencies of *PARK2* DNA copy number changes were plotted using a polar histogram. The OncoPrint cancer profiling database was used to analyze *PARK2* mRNA expression across 13,499 cancerous and 2,708 normal tissue specimens from 125 independent microarray datasets representing 27 different cancer types. The degree of *PARK2* mRNA underexpression (≥ 0.5 and ≥ 1 -log₂-fold change in tumor versus normal) was plotted across all tumor types. Kaplan-meier analysis in Figure S1C was performed using the KM plotter (Szasz et al., 2016). Student t-test and one- or two-way Anova were used to evaluate the statistical significance among different variables as indicated in the respective figure legends, *P*: n.s. (not significant), * ($P < 0.05$), ** ($P < 0.01$).

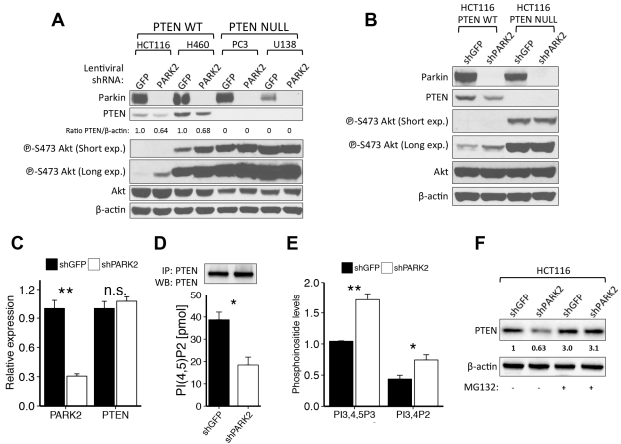
Supplemental Information

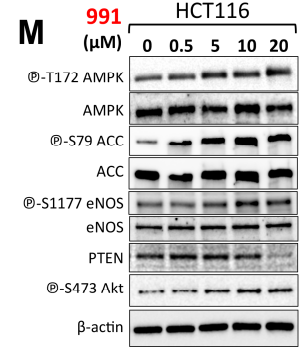
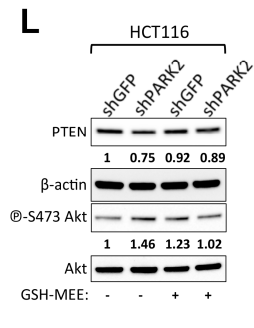
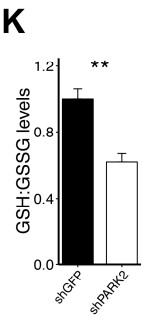
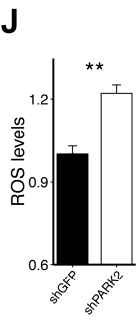
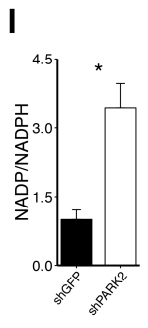
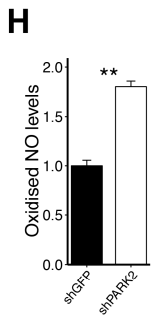
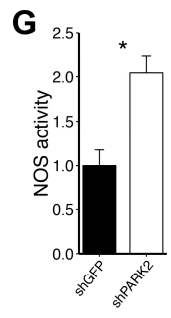
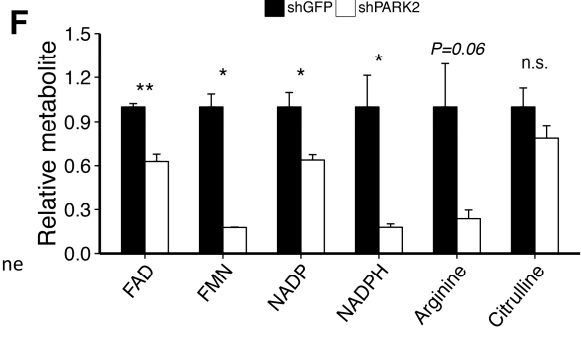
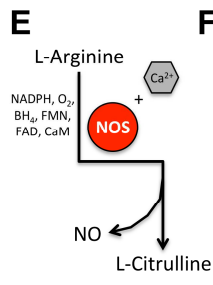
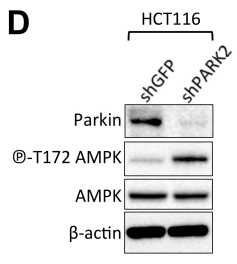
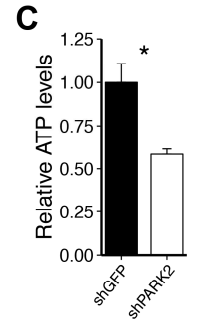
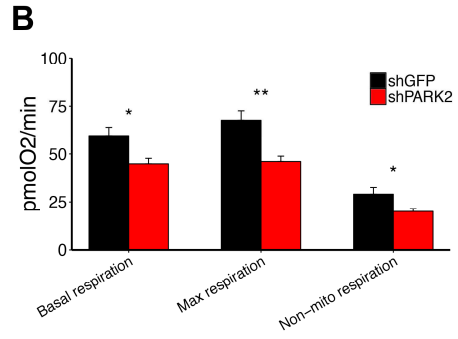
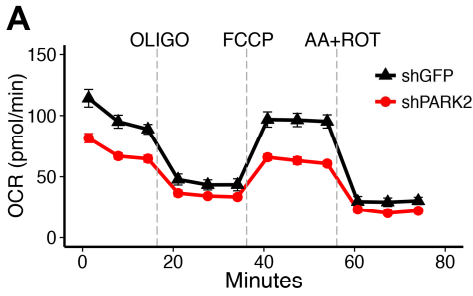
Document S1. Tables S1 and S2

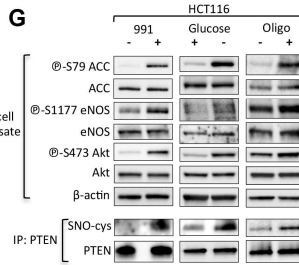
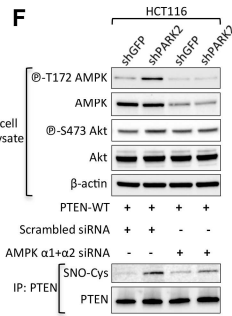
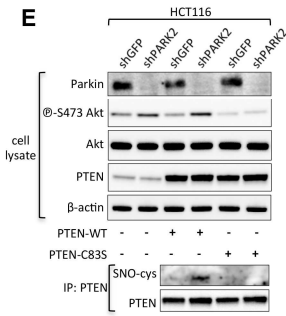
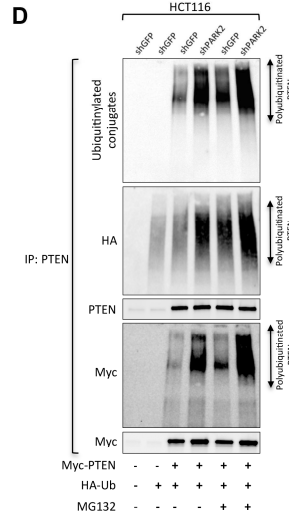
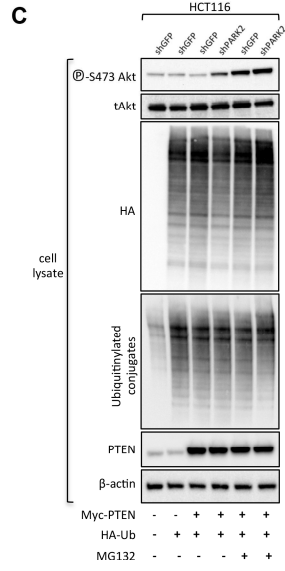
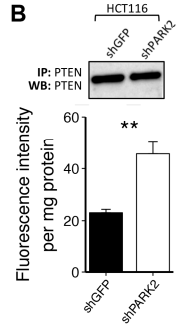
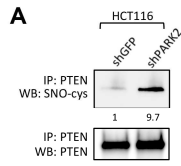


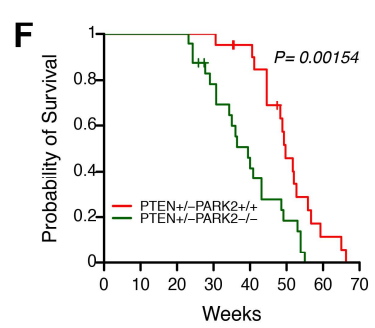
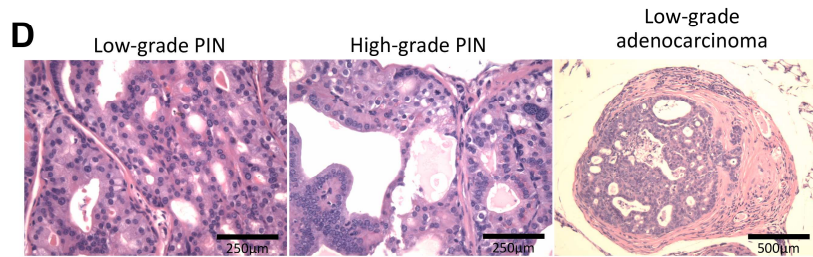
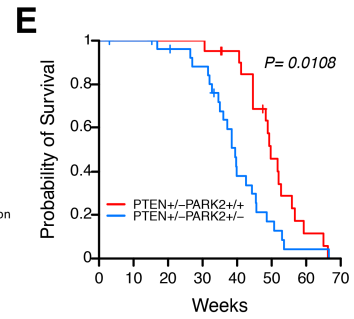
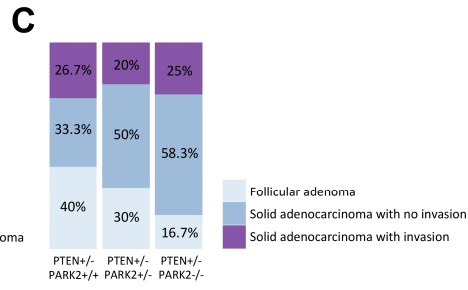
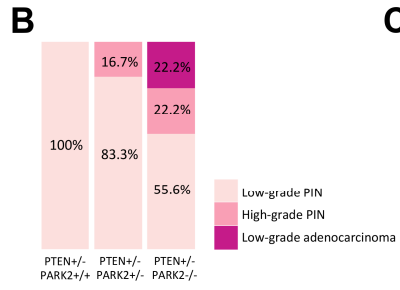
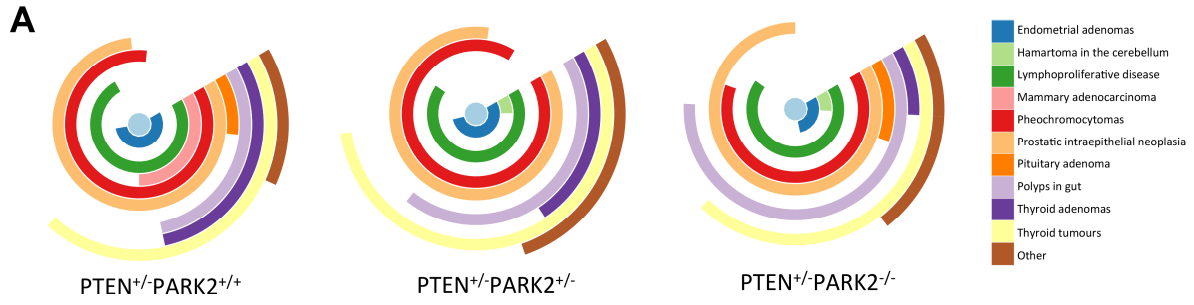












The NIHMS has received the file 'Supplemental Information.pdf' as supplementary data. The file will not appear in this PDF Receipt, but it will be linked to the web version of your manuscript.

The NIHMS has received the file 'Supplemental table 1.xlsx' as supplementary data. The file will not appear in this PDF Receipt, but it will be linked to the web version of your manuscript.

The NIHMS has received the file 'Supplemental table 2.xlsx' as supplementary data. The file will not appear in this PDF Receipt, but it will be linked to the web version of your manuscript.